W. W. Hansen Experimental Physics Laboratory

STANFORD UNIVERSITY
STANFORD, CALIFORNIA 94305 - 4085

Gravity Probe B Relativity Mission

S0898

VERIFICATION OF KNOWLEDGE OF PROPER MOTION OF THE EFFECTIVE GUIDE POINT

October 20, 2003

Prepared by: Michael Ratner 10/24/2003 Michael Ratner Date Harvard-Smithsonian Center for Astrophysics, Guide Star Lead Scientist	Prepared by: Jeff Kolodziejczak 10/20/03 Jeff Kolodziejczak Date NASA/MSFC, Project Scientist
Approved by: Richard Whelan 10/28/03 Richard Whelan Date Gravity Probe B Systems Engineering	Approved by: George "Mac" Keiser 10/31/03 George "Mac" Keiser Date Stanford University Gravity Probe B Chief Scientist
Approved by: Irwin Shapiro 10/27/03 Irwin I. Shapiro Date Harvard-Smithsonian Center for Astrophysics, Guide Star Principal Investigator	Approved by: Dorrene Ross FOR 10/29/03 Dorrene Ross Date Stanford University Gravity Probe B Quality Assurance
	Approved by: C. W. Francis Everitt 10/29/2003 C. W. Francis Everitt Date Principal Investigator

ITAR Assessment Performed BBFree for Tom Langenstein ITAR Control Req'd? ☐ Yes ☒ No

TABLE OF CONTENTS

CHANGE RECORD ..... **II**

TABLE OF CONTENTS ..... **IIIII**

LIST OF ACRONYMS, ABBREVIATIONS AND SYMBOLS ..... **V**

LIST OF TABLES ..... **VI**

LIST OF FIGURES ..... **VII**

1. SUMMARY **1**

2. INTRODUCTION **2**

2.1 T002 REQUIREMENT 2
2.2 T003 REQUIREMENT 3

3. VERIFICATION OF KNOWLEDGE OF EFFECTIVE GUIDE-POINT PROPER MOTION REQUIREMENTS **3**

3.1 EFFECTIVE GUIDE-POINT PROPER MOTION (T002 – REQUIREMENT 3) 3
3.2 DIFFERENCE BETWEEN EFFECTIVE GUIDE-POINT AND VLBI PROPER MOTIONS (T003 – REQUIREMENT 25.4.2) 4
3.2.1 DIFFERENCE BETWEEN OPTICAL CENTROID AND EFFECTIVE GUIDE POINT PROPER MOTIONS 4
3.2.1.1 GUIDE STAR VARIABILITY COMBINED WITH MEASURED NEBULOSITY 5
3.2.1.1.1 STATISTICAL UNCERTAINTY 6
3.2.1.1.2 UNKNOWN BIAS 6
3.2.1.2 GUIDE STAR VARIABILITY COMBINED WITH NEBULOSITY 6
3.2.1.2.1 MOLECULAR CLOUD 6
3.2.1.2.2 DUST 7
3.2.1.2.2 GUIDE STAR LOCAL NEBULA 8
3.2.1.3 GUIDE STAR VARIABILITY COMBINED WITH OTHER STARS 8
3.2.1.3.1 KNOWN STARS 8
3.2.1.3.2 UNKNOWN STARS 9
3.2.1.4 GUIDE STAR COMBINED WITH OTHER STAR VARIABILITY 9
3.2.1.4.1 KNOWN STARS 10
3.2.1.4.2 UNKNOWN STARS 10
3.2.1.5 ZODIACAL LIGHT 10
3.2.2 DIFFERENCE BETWEEN VLBI AND OPTICAL CENTROID PROPER MOTIONS 11
3.2.2.1 CHANGES IN STAR SPOTS 11
3.2.2.2 RADIO SOURCE DRIFT WITH RESPECT TO STAR SURFACE 12
3.2.2.3 UNRESOLVED THIRD BODY 12
3.2.2.4 VARIATION OF PRIMARY/SECONDARY BRIGHTNESS RATIO 13
3.2.2.5 FLARES AND OTHER TRANSIENT EVENTS 14

REFERENCES **15**

APPENDICES **1**

APPENDIX A – TREE-DIAGRAMS OF ERROR TERMS. (JJK) 1
APPENDIX B – GUIDELINES FOR BOXES UNDER ERROR TREE ITEM 3.1 1
APPENDIX C – GLOSSARY 1
APPENDIX D – PROPER MOTION OF THE EFFECTIVE GUIDE POINT RESULTING FROM GUIDE STAR VARIABILITY COMBINED WITH OTHER SOURCES IN THE GP-B TELESCOPE FIELD OF VIEW.(JJK) 1
APPENDIX E – CONSTRAINTS ON NEBULOSITY NEAR IM PEG FROM ANALYSIS OF HST IMAGES. (JJK) 1
APPENDIX F – CONSTRAINTS ON NEBULOSITY NEAR IM PEG FROM (OTHER-THAN-HST) OBSERVATIONS AND THEORETICAL CONSIDERATIONS. (MIR) 1

APPENDIX G – A CATALOG OF STARS NEAR IM PEG AND CONSTRAINTS ON UNKNOWN SOURCES. (JJK)..... 1
APPENDIX H – CONSTRAINTS ON VARIABILITY OF SOURCES (OTHER THAN IM PEG) IN THE TELESCOPE FIELD-OF-VIEW FROM OBSERVATIONS AND THEORETICAL CONSIDERATIONS.(MIR) 1
APPENDIX L – PLANNED OPTICAL OBSERVATIONS AND ANALYSES (MIR) 1
APPENDIX M – CONSTRAINTS ON THE DIFFERENCE BETWEEN RADIO AND OPTICAL PROPER MOTION FROM OBSERVATIONAL AND THEORETICAL CONSIDERATIONS. (MIR)..... 1

LIST OF ACRONYMS, ABBREVIATIONS AND SYMBOLS

B,V,R,I	astronomical magnitudes associated with specific wavelength bands
CCD	Charge-coupled device
CDF	Cumulative distribution function
Dec	declination
EGP	Effective guide point
FOV	Field of view
FWHM	Full Width at Half Maximum
FWHM	Full width at half maximum
Ghz	gigahertz
GSV	Guide star valid
HST	Hubble Space Telescope
IM Peg	GP-B Guide Star (=HR8703)
mag	astronomical magnitudes
marcsec	milliarcseconds
mas	milliarcseconds
PC	Planetary Camera CCD of WFPC2
PRF	Point response function
PSF	Point spread function
RA	Right ascension
RS CVn	Variable star and variable star type
RSS	Root Sum of Squares
ST	Spacecraft science telescope
VLBI	Very Long Baseline Interferometer
VRC	Virtual Reseach Center
WF	Wide field CCDs of WFPC2
WFPC2	Wide Field Planetary Camera 2

LIST OF TABLES

Table 1-1 Requirements
Table 1-2 Mitigations for low-probability potential unknowns
Table D-1 Properties required for color corrected i_{os}/i_{gs}
Table D-2 Color relationships for normal, stars for BVRI and Palomar Plate O and E
Table D-3 Spatially averaged nebulosity imbalance to produce a 0.1 mas/yr proper motion component
Table E-1 Estimated limits of nebulosity gradient accuracy from HST images due to potential systematic errors resulting from bias variations on WFPC2 WF CCDs
Table E-2 Results of HST nebulosity analysis
Table G-1 Catalog of stars with 100 arcsec of IM Peg
Table G-2 1-σ upper bounds for other stars near IM Peg from HST images
Table L-1 Summary of planned optical observations
Table L-2 Planned analyses

LIST OF FIGURES

Figure A-1 Top level error tree.
Figure A-2 Error tree components for the difference between effective guide point proper motion and optical centroid proper motion.
Figure A-3 Error tree components for the difference between VLBI proper motion and optical centroid proper motion.
Figure D-1 GP-B telescope conceptual elements referenced in text.
Figure D-2 Pointing bias, δ, resulting from another star in the field of view (schematic).
Figure D-3 Roll-angle dependence of pointing bias.
Figure D-4 Roll-averaged vignetting factor across the edge of the field of view.
Figure D-5 Statistical analysis of the variation in flux from HR 8703.
Figure D-6 Effects of spectral type on pointing bias.
Figure D-7 V magnitude required to produce an effective guide point proper motion of 0.1 mas/yr, assuming a plausible flux variation of 5% per year
Figure D-8 Required V magnitude for an additional star with B-V = 0 to produce a 0.1 mas/yr proper motion of the effective guide point

LIST OF APPENDICES

A. Tree-diagram of error terms.
B. Guidelines for boxes under error tree item 3.1.
C. Glossary.
D. Proper motion of the effective guide point resulting from guide star variability combined with other stars in the GP-B telescope field-of-view.
E. Constraints on nebulosity near IM Peg from analysis of HST images.
F. Constraints on nebulosity near IM Peg from (other-than-HST) observations and theoretical considerations.
G. A catalog of stars near IM Peg and constraints on unknown sources.
H. Constraints on variability of sources in the telescope field-of-view other than IM Peg from observations and theoretical considerations.
I. deleted before release (was “Proper Motion from Optical Observations”, deleted because optical proper motion and proper acceleration limits are too large to constrain GP-B uncertainty)
J. deleted before release (was “Uncertainty in extragalactic reference star correspondence to inertial space”, deleted because error is already accounted for as an unknown bias in the VLBI error term (see S0890))
K. deleted before release (was Proper Motion Uncertainty from VLBI Observations of IM Peg, moved to S0890 (Ratner, 2003))
L. Planned optical observations and analyses
M. Constraints on the difference between radio and optical proper motion from theoretical considerations.

1. SUMMARY

This document verifies T002 requirement 3 and T003 requirement 25.4.2, which are the requirements on knowledge of the proper motion of the effective guide point (EGP). Recently, a task was undertaken to identify potential low-probability error terms, which if unmitigated, would lead to larger-than-expected high-confidence (>3σ) intervals for the proper motion. The result of this analysis is included in the appendices. The verification is based on known error terms and mitigation plans for addressing the identified low-probability potential unknowns. Table 1-1 summarizes the (1σ) uncertainty based on known error terms. Table 1-2 summarizes the mitigations for low-probability potential unknowns.

Table 1-1. Requirements

Requirement	Specification	Value	Pass
T003 Requirement 25.4.2	< 0.05 mas/yr	0.045 mas/yr	Yes
T002 Requirement 3	<0.15 mas/yr	0.11 mas/yr	Yes

Table 1-2. Mitigations for low-probability potential unknowns (See Appendix L for details of planned observations and analysis)

Improbable Potential Unknowns	Mitigations
Proper motion error due to an undetected third body.	• Probabilistic Monte Carlo analysis of errors given constraints from observed source limits. • U. Pittsburgh optical astrometric observations • Lick Obs. spectroscopic observations
Nebulosity due to an undetected nearby dust sheet.	• U. Hawaii deep occulted CCD imaging • Lick Obs. polarization observations • Complete analysis of in-hand adaptive optics images
Large changes in star spots	• Doppler-imaging spectroscopic observations
Unusual variability of other sources in the field of view	• USNO (Flagstaff) photometric observations • U. Pittsburg photometric observations
Unusual variability of guide star	• Fairborn Obs. photometric observations • Tennessee State U. photometric observations • AAVSO photometric observations

This verification is rather complex in part because the requirement is so small. It is instructive to note that 0.05 mas/yr corresponds to a velocity of about 30 m/s at the 100 parsec distance of IM Peg. The logic of the verification 25.4.2 goes as follows:

- Analyses are used to derive the error tree terms based on previous observations and astrophysical probabilities. These lead to the projected uncertainty.
- Planned observations are used to validate the analyses and conclusions from previous observations by addressing improbable cases where the error terms

depend directly on events which might occur during the mission or to supply bounds to increase confidence that none of the improbable cases are the real case (in other words, to better constrain the probabilities of improbable cases).

We show that the projected uncertainty is within errors. Where there is a possibility that something could change during the mission, we show that observations are planned with adequate sensitivity to detect the change. Where there is a possibility that, if one of our probabilistic assumptions was unlucky, then an error could be larger than we estimate, we show that observations and analyses are planned with adequate sensitivity to improve our confidence in the assumption.

2. INTRODUCTION

This analysis document provides verification of the T002 requirement "3 Proper Motion" which is quoted in section 2.1, and verification of the related T003 requirement "25.4.2 Motion of Effective Guide Point Relative to Radio Centroid," which is quoted in section 2.2. The related T003 requirement "25.4.1 Proper Motion of Radio Centroid" is not discussed in detail here but is verified in (Ratner & Kolodziejczak, 2003) with value 0.10 marcsec/year. Section 3 summarizes the more detailed discussion contained in the appendices, providing values for the various contributions to the motion of the EGP relative to the VLBI-measured radio centroid. For reference, Schultz (1998) provides the rationale for selection of IM Peg (=HR 8703) as the GP-B guide star.

2.1 T002 Requirement

3 Proper Motion

"The projected uncertainty in the proper motion of the effective guide point at the mid-point of the GP-B science data collection period shall be less than 0.15 marcsec/year in declination and right ascension times cosine of declination."

Note: The proper motion validity will be confirmed by performing suitable astronomical observations and analyses, which are likely to reduce the width of the 99.9% confidence interval for the measured value.

The proper motion of the effective guide point is the rate of secular change in the direction of the ST line-of-sight resulting from motion of the guide star with respect to the solar system barycenter and from changes in the properties of the guide star or of discrete or diffuse astronomical sources of optical and near infrared light in the ST field of view. It is composed of the proper motion of the optical centroid of all unresolved objects, which compose the guide star and additional secular drift associated with relative variations in position, intensity and color among any of the luminous objects in the ST field of view.

The proper motion uncertainty critical to the mission is that of the best estimate that will be available, about 1 year after the end-of-mission, of the proper motion at the midpoint

of the span of science data. The projected uncertainty in proper motion is the uncertainty of that estimate, derived prior to launch and based on conservative assumptions regarding the success of all existing or planned observations whose analysis is not yet complete.

2.2 T003 Requirement

25.4.2 Motion of Effective Guide Point Relative to Radio Centroid
"Prior to launch, additional observations and analyses shall be planned to ensure that the projected uncertainty in the difference, during the GP-B data collection period, between the effective guide point and the radio centroid proper motions is less than 0.05 marcsec/year (1 sigma) in declination and right ascension times declination, where projected uncertainty is interpreted in the context of T002 requirement #3 and specifically defined in the last sentence of the fourth paragraph thereof."

Comment: The goal of these additional observations and analyses is to reduce the 99.9% confidence interval for the proper motion.

3. VERIFICATION OF KNOWLEDGE OF EFFECTIVE GUIDE-POINT PROPER MOTION REQUIREMENTS

3.1 Effective Guide-Point Proper Motion (T002 – Requirement 3)

GP-B gyroscope drift rate is measured relative to a specific reference which we call the experiment's *effective guide point* (EGP). In Appendix A, figures A-1, A-2 and A-3 define an error tree with a series of boxes accounting for the various possible error sources. The box associated with this error term accounts for uncertainty in the annual drift in celestial coordinates of the EGP. The EGP for the GP-B experiment is determined by the detected light in the science telescope (ST) field of view (FOV). The dominant source of light in the FOV is the guide star, IM Peg (HR 8703). The luminosity of IM Peg is variable. If the ST FOV contained only the guide star, or if other sources of light in the field of view amounted to a uniform background vs. celestial position, then the proper motion of GP-B's effective guide point would be the same as the proper motion of the guide star. The uncertainty in the GP-B effective guide point would then depend only on the uncertainty in the difference between the VLBI-determined proper motion and the optical centroid proper motion (sec. 3.2.2), combined with the uncertainty in the VLBI-determined proper motion. The later was verified to be 0.1 mas/yr based on (Ratner & Kolodziejczak, 2003). However, if the light from other sources in the ST FOV is both non-zero and non-uniform as a function of celestial position, then the GP-B effective guide point proper motion may differ from the guide star optical centroid proper motion and an additional error term must be included to account for uncertainty in this difference (sec. 3.2.1). The three error terms are largely independent. The 1σ uncertainty is derived from the root-sum-of-squares of the two plausible terms:

EW – 1 σ	0.11mas/yr
NS – 1 σ	0.11 mas/yr

3.2 Difference between Effective Guide-Point and VLBI Proper Motions (T003 – Requirement 25.4.2)

The error-tree box in the Appendix A, Figure A-1, corresponding to this error term accounts for the difference between the VLBI-measured proper motion and the EGP proper motion. The sources of error that contribute to this box fall into two categories:

1. Those that contribute to the difference between the guide star optical centroid proper motion and the EGP proper motion (sec. 3.2.1).
2. Those that contribute to the difference between the guide star optical centroid proper motion and the VLBI-measured proper motion (sec. 3.2.2).

The values are derived from the root-sum-of-squares of these two plausible terms.

EW – 1 σ	0.045 mas/yr
NS – 1 σ	0.038 mas/yr

3.2.1 Difference between Optical Centroid and Effective Guide Point Proper Motions

This box accounts for the possibility that the experiment's effective guide point proper motion may differ from the guide star proper motion. Figure A-2 shows the details of the tree structure, which composes this box. During the science experiment, the GP-B attitude and translation control (ATC) system will use the ST signal to orient the space vehicle. The orientation is adjusted to null the difference in signals from detectors, which receive light from opposite sides of a roof prism at the telescope focus. If the light distribution as a function of celestial coordinates in the ST FOV changes, then the orientation of the space vehicle, averaged over an appropriate time scale, may also change. Conceptually, we define the *detected photon flux imbalance* of any one of the four ST detector pairs, due to light sources other than the guide star, as the difference between the amounts of light from these sources detected by the two detectors (+ and -). At any given roll angle the ST detectors are affected by the imbalance in light on either side of the two nearly orthogonal lines on the sky passing through the guide star and lying parallel to the edges of the x and y axis roof prisms. If the detected photon flux imbalance is non-zero, then a variation in the guide star luminosity will produce a change in the space vehicle orientation. If the detected photon flux imbalance is itself variable, then a change in the space vehicle orientation will result, independent of the guide star luminosity variation. A detected photon flux imbalance may be caused by the distribution of other stars in the ST FOV and spatial variations in diffuse light, or nebulosity, within the ST FOV. Zodiacal light is a known type of nebulosity, which varies over a year, so we define it as a separate error term. We therefore have four error terms, which are

combined to determine the uncertainty in the difference between the effective guide point and the guide star optical centroid proper motion:

1. combined effect of guide star variability and nebulosity
2. combined effect of guide star variability and other stars
3. effect of any variability of the other star
4. combined effect of guide star variability and zodiacal light

Item 1 is derived by two independent methods: 1a) direct measurement of a nebulosity gradient from observations, and 1b) nebulosity constraints deduced from indirect measurements, and statistical and theoretical considerations. The value is determined by taking the root-sum-of-squares of the minimum of plausible values for 1a and 1b combined with plausible values for items 2, 3, and 4.

The projected values for three of these terms depend on the linear term of guide star variability. Appendix D shows this to be less than 5% at the 1-sigma level. There is a small possibility that the linear trend in the guide star's brightness during the mission may be significantly larger than this, and if it were not measured, the error associated with these three terms may be larger than estimated here. For this reason, observations will be performed to monitor the guide star variability as shown below and in Appendix L. These observations should determine any linear term in the guide star brightness to 1-3%/yr, which will allow a partial correction for the known effects, if necessary.

EW – 1 σ	0.030 mas/yr
NS – 1 σ	0.017 mas/yr

Improbable Potential Unknowns	**Mitigations**
Unusual variability of guide star	• Fairborn Obs. photometric observations • Tennessee State U. photometric observations • AAVSO photometric observations

3.2.1.1 Guide star variability combined with measured nebulosity

This box accounts for the possibility that the experiment's effective guide point proper motion may differ from the guide star proper motion because of the combined effects of guide star variability and nebulosity, based on constraints on nebulosity derived from direct observations. The HST images taken in 1997 provide useful observational constraints on nebulosity near IM Peg. An analysis of these images is described in Appendix E. The plausible-case errors are determined by taking the root-sum-of-squares of the corresponding statistical uncertainty and unknown bias terms.

EW – 1 σ	0.07 mas/yr
NS – 1 σ	0.07 mas/yr

3.2.1.1.1 Statistical Uncertainty

This box accounts for the statistical uncertainty, which arises from the HST image analysis of Appendix E. We apply this error at 45° to North, by assigning $1/\sqrt{2}$ times the total error to each component (the measured gradient was ~45 degrees NE/SW).

EW – 1 σ	0.05 mas/yr
NS – 1 σ	0.05 mas/yr

3.2.1.1.2 Unknown Bias

This box accounts for sources of unknown bias associated with the HST image analysis of Appendix E. This has the same magnitude as the statistical uncertainty term because the is consistent with the bias variations in the HST images. We apportion this error equally between the two Cartesian components, by assigning $1/\sqrt{2}$ times the total error to each component.

EW – 1 σ	0.05 mas/yr
NS – 1 σ	0.05 mas/yr

3.2.1.2 Guide star variability combined with nebulosity

This box accounts for the possibility that the experiment's effective guide point proper motion may differ from the guide star proper motion because of the combined effects of guide star variability and nebulosity, based on constraints on nebulosity derived from indirect observations and theoretical considerations. Specific analyses and detailed discussion for the contributing items are included in Appendix F. The plausible case is determined by taking the root-sum-of-squares of the various phenomenological terms below.

EW – 1 σ	0.016 mas/yr
NS – 1 σ	0.016 mas/yr

3.2.1.2.1 Molecular Cloud

Molecular clouds are hierarchically fragmented but highly localized regions of the interstellar medium characterized by unusually high densities of gas and dust. The largest molecular cloud complexes are about 50 pc in size and separated by about 500 pc (Mathis 2000). There is no reason to believe that a molecular cloud lies along the line of sight to IM Peg. To the contrary, maps of the 115 GHz emission of the CO molecule reveal no CO within 1° of IM Peg (see Appendix F, section 6). The plausible error is due to dense clouds is zero.

EW – 1 σ	0.0 mas/yr
NS – 1 σ	0.0 mas/yr

3.2.1.2.2 Dust

This box accounts for the possibility that the experiment's effective guide point proper motion may differ from the guide star proper motion because of the combined effects of guide star variability and scattered light from interstellar dust grains. A low-probability potential unknown is identified from the worst-case analysis of Appendix F. It is based on the following:

- A mapping of ISM dust indicates that the extinction coefficient due to dust in the general direction of IM Peg is nearly 20%. We assume an albedo of 0.5 for the dust, which means that half of the extinction is due to absorption and half due to scattering.
- The distance to IM Peg places it near the edge of the local bubble. This increases the probability that much of the dust may be radially collocated with IM Peg.
- A simple thin-sheet dust model suggests that under reasonable worst-case assumptions, the light scattered toward Earth could produce a detected photon flux imbalance as large as 1.4% of the detected photon flux from the guide star. The worst-case error is based on conservative assumptions concerning the thickness of the dust sheet, its distance from the guide star and its angle of inclination to the line of sight.
- A 5%/yr variation in the guide star flux is assumed.

Sections 1, 3, and 4 of Appendix F contain detailed discussion of these points. The plausible error is small because the detected flux from dust falls off roughly as the inverse of dustsheet thickness and as the inverse square of the distance between the sheet and the guide star. The dominant source of nebulosity imbalance changes from the inclination angle of the dust sheet to its density variation across the field of view. This low-probability potential unknown will be mitigated by planned observations and analysis of existing data. The sensitivity of these observations is ~24^{th} mag/arcsec^2, which should constrain the error to 0.03 mas/yr based on the analysis in Appendix D. Appendix L provides more detail on the planned observations and analyses.

EW – 1 σ	0.01 mas/yr
NS – 1 σ	0.01 mas/yr

Improbable Potential Unknown	Mitigation
Nebulosity due to an undetected nearby dust sheet.	• U. Hawaii deep occulted observations • Lick Obs. polarization observations • Complete analysis of in-hand coronographic data

3.2.1.2.2 Guide Star Local Nebula

This box accounts for the possibility that the experiment's effective guide point proper motion may differ from the guide star proper motion because of the combined effects of guide star variability and (possibly variable) light scattered by local dust in the IM Peg system. The plausible case is based on inconsistent evidence for an infrared excess, which, if real, would likely be the result of dust. The plausible case is based on the conservative assumption that the infrared excess is real and a result of absorption and thermal re-emission by dust with an albedo of 0.5, which implies a $\sim 10^{-4}$ mean ratio of dust to star brightness in the optical range. A 5%/yr variation of that ratio is also assumed. See sections 2 and 5 of Appendix F for a more detailed discussion. We apportion this error equally between the two Cartesian components, by assigning $1/\sqrt{2}$ times the total error to each component.

EW – 1 σ	0.012 mas/yr
NS – 1 σ	0.012 mas/yr

3.2.1.3 Guide star variability combined with other stars

This box accounts for the possibility that the experiment's effective guide point proper motion may differ from the guide star proper motion because of the combined effects of guide star variability and other stars. Appendix D provides the relationships between a star's position, magnitude and color and the component of effective guide point proper motion the star introduces. Appendix D also provides an estimate of guide star variability based on observed behavior. The plausible-case errors are determined by taking the root-sum-of-squares of the terms derived for known stars and unknown stars below.

EW – 1 σ	0.025 mas/yr
NS – 1 σ	0.005 mas/yr

3.2.1.3.1 Known Stars

Appendix G contains a table of all known stars within 100 arcsec of IM Peg. The table was compiled from a search of existing catalogs as well as detected stars from the HST images of IM Peg. A value for effective guide point proper motion is tabulated for each star following the recipe given in appendix D assuming the plausible 5% guide star variability. The EW and NS components of these individual terms are summed to give the respective plausible cases. This box is only an error because we are assuming the guide star variability is unknown. Once the guide star variability is known, this becomes a correction to the proper motion of the effective guide point.

EW – 1 σ	0.025 mas/yr
NS – 1 σ	0.005 mas/yr

3.2.1.3.2 Unknown Stars

Appendix G also contains an analysis of constraints on unknown stars in the field of view. These constraints are based on analysis of HST images and probabilistic arguments regarding unresolved sources. The existence of an unknown third body, which is part of the guide star system, is accounted for in sec. 3.2.2.3. It is improbable ($p << 0.3$) that a significant unknown source exists that has not been detected.

EW – 1 σ	0.00 mas/yr
NS – 1 σ	0.00 mas/yr

3.2.1.4 Guide star combined with other star variability

This box accounts for the possibility that the experiment's effective guide point proper motion may differ from the guide star proper motion because of the combined effects of the guide star and variability of other sources. Appendix D provides the relationships between a star's position, magnitude and color and the component of effective guide point proper motion the star introduces. Appendix H provides an estimate of the plausible-case other-star variability based on observational and statistical considerations. The plausible-case errors are determined by taking the root-sum-of-squares of the terms derived for known stars and unknown stars below. There is a small possibility that a star in the field of view could become significantly brighter during the GP-B mission. If this were to occur than the error estimate below would be incorrect. For this reason, we plan to perform a series of observations to monitor the variability of other stars near IM Peg. These observations, accurate to <0.1 magnitudes, will be adequate to allow us to correct for errors at <0.01 mas/yr level if variability is detected in another source in the GP-B ST FOV based on analyses in Appendices D and G.

EW – 1 σ	0.0001 mas/yr
NS – 1 σ	0.0001 mas/yr

Improbable Potential Unknowns	**Mitigations**
Unusual variability of other sources in the field of view	• USNO (Flagstaff) photometric observations • U. Pittsburg photometric observations

3.2.1.4.1 Known Stars

We compute the entries for this box based upon the measured magnitudes and estimated bounds on variability of the stars within 75" of the guide star, and the calculations given in appendix D. The plausible case, accounting for measured variability of statistical populations of stars, is based on a typical variation of 0.001 mag/yr for a star with I magnitude of 14.1. The effects are equally apportioned in the EW and NS direction. Appendix H details the rationale.

EW – 1 σ	0.0001 mas/yr
NS – 1 σ	0.0001 mas/yr

3.2.1.4.2 Unknown Stars

At distances from the guide star ≥ 26", we expect that all undetected stars are (currently) dimmer than the known stars. When stars have been detected by one technique but not another, it has generally been either because they were fainter or closer to the guide star than those detected by the other technique. There are two scenarios in which a still unknown star could contribute a plausible-case error as large or larger than those included in 3.2.1.4.1: Either the unknown star is brighter and undetected only because it is closer to the guide star, or else it is now fainter, but could brighten more dramatically than the 0.1 mag/yr allowed for the known stars. Most of the region within 26" of the guide star is covered by our Hubble Space Telescope (HST) images of the field around the guide star through various band filters. However, there is a region close to the guide star in which the limiting magnitude of all the images is brighter than that of the known stars. Stars brighter than 15th V-magnitude can be ruled only at distances ≥ 0.5".

EW – 1 σ	0 mas/yr
NS – 1 σ	0 mas/yr

3.2.1.5 Zodiacal Light

This box accounts for uncertainty in the guide star proper motion resulting from variability in the guide star intensity combined with the diffuse gradient of light intensity resulting from zodiacal light.

J. Goebel (2001) indicates that the maximum gradient in zodiacal light that the GP-B telescope will observe produces a 0.0143 mas displacement in the telescope pointing direction. This maximum, combined with a plausible 5%/yr variation in guide star brightness, yields a plausible limit of <0.001 mas/yr on the zodiacal light contribution to the difference between the effective guide point and the guide star optical centroid. The maximum gradient is in the direction normal to the ecliptic plane, inclined about 23° to the NS direction, so the above limit is approximately applicable. In the EW direction, the

largest gradient that the GP-B telescope will see is about half as large as the NS direction. The values below reflect this. Depending upon the seasonal timing of the mission, the expected errors would be further reduced below these already negligible values due to the annual cycle of the relative position of the Sun and the guide star. The year-to-year variation of the brightness of the Sun is negligible in comparison to that of IM Peg (see, *e.g.*, Shatten and Orosz 1999).

EW – 1 σ	0.0005 mas/yr
NS – 1 σ	0.001 mas/yr

3.2.2 Difference between VLBI and Optical Centroid Proper Motions

This box accounts for uncertainty in the difference between radio and optical proper motions deduced from indirect measurements, and statistical and theoretical considerations. Figure A-3 shows the details of the tree structure, which composes this box. We take the root-sum-of-squares of the several expected contributions, as if they were uncorrelated. Although the various correlations are unknown, since none of them is expected to be large, and since each could be negative as well as positive, this procedure is reasonable.

EW – 1 σ	0.034 mas/yr
NS – 1 σ	0.034 mas/yr

3.2.2.1 Changes in star spots

Berdyugina *et al.* (2000) present images (Doppler maps) of the surface of IM Peg based on spectroscopic data. These maps show the existence of large spots, which vary in size and position. Such variation may cause the optical centroid to drift with respect to the center of the disk of the primary star. Appendix M includes a table of eight rotation-averaged centroid offsets based on their data, which span 3 years. For our plausible but conservative case, we assume that during the ~1 yr mission the centroid will drift across the entire range of positions inferred from the 3 yr span of spectroscopic data. For each component we reduce the resulting value by $\sqrt{2}$. While it is unlikely that star spot changes will produce an error which is significantly larger than this, the possibility of a >0.05mas/yr drift cannot be ruled out without additional observations during the GP-B mission. For this reason, a series of Doppler images are planned over the time span of the mission.

EW – 1 σ	0.017 mas/yr
NS – 1 σ	0.017 mas/yr

Improbable Potential Unknowns	Mitigations
Large changes in star spots	• Doppler-imaging spectroscopic observations

3.2.2.2 Radio source drift with respect to star surface

We compute the entries for this box based upon plausible estimates for the maximum rate of displacement of the radio emission centroid from the center of mass of the primary star of the IM Peg binary system. The plausible case allows for a sinusoidal motion of the mean position of the radio centroid with a projected peak-to-peak displacement of up to 0.34 mas, or one-fourth the stellar diameter, and a period of 20 years. Such a motion could account for latitudinal drifts in features of the primary star associated with a decades-long magnetic cycle. The effects are equally apportioned to the EW and NS directions. Appendix M details the rationale.

EW – 1 σ	0.03 mas/yr
NS – 1 σ	0.03 mas/yr

3.2.2.3 Unresolved third body

This box accounts for the errors that could be introduced by conceivable third stars or planets in orbit around the IM Peg binary system. However, no evidence exists for such a body in either the composite spectrum of IM Peg or the inferred radial velocity of its primary. It is quite common for star systems with at least two components to also contain a third. The plausible limit of zero is based on the analysis of observational constraints on the IM Peg system that has been performed, using Monte Carlo techniques, by Chandler & Ratner (2003), which indicates that it is implausible that a third component exists, even at levels below current detection limits. Nevertheless, a third component is not ruled out. This possibility creates an improbable potential error, for which the probability of exceeding 0.05 mas/yr is estimated to be below 0.3%.

Observations are planned to continue to increase our ability to detect a third body by looking for its effects on radial velocity derived from spectroscopic measurements, and motional effects derived from astrometric optical observations. Constraints derived from these observations can be folded into the Monte Carlo study to improve our confidence in this error term.

EW – 1 σ	0.00 mas/yr
NS – 1 σ	0.00 mas/yr

Improbable Potential Unknowns	**Mitigations**
Large undetected offset of EGP proper motion from VLBI proper motion due to an unknown third body.	• Probabilistic Monte Carlo analysis of errors, given constraints from observed source limits. • U. Pittsburgh optical astrometric observations • Lick Obs. Spectroscopic observations

3.2.2.4 Variation of primary/secondary brightness ratio

Several factors suggest that this term must be very small.

The lack of evidence of the secondary in the spectrum of IM Peg suggests that it is at least three magnitudes fainter than the primary over much of the visible spectrum. For reasonable values of the mass of the primary, the maximum separation on the sky of the two components is only 3-4 mas. At such distances, the images nearly completely overlap and the instantaneous guide point will be near the instantaneous centroid of the light from the two components. Thus the maximum instantaneous astrometric pointing bias away from the center of the primary due to the secondary is only <~0.3 mas. In any case, this offset is periodic with a known 24.65 day period, and would merely cancel a small part of the periodic motion of the EGP due to the orbit of the primary, a motion that is to be estimated in the GP-B data analysis.

Further, the very-low-eccentricity orbit of each component will project on the sky as an ellipse centered on the center of mass of the binary. Consequently, departure of the orbit-averaged centroid position from that center of mass depends on changes of the brightness ratio of the two stars within a single orbit period. Moreover, if that ratio changes at a constant rate, the offset will be nearly identical for each orbit, and hence yield a drift in the orbit-averaged guide point that is second order in the rate of brightness ratio change. More realistically, an offset in the proper motion of the EGP will be dependent on departures from a constant rate of change. At least another order of magnitude decrease can be expected. Finally, if by analogy with the long term photometric behavior of IM Peg, we allow for the plausible case a variation of only 5%/yr in the orbit-averaged offset, we find an upper bound on the plausible error of 0.0015 mas/yr.

This error is along the major axis of the projected orbit ellipses; the perpendicular error is at least a factor of two smaller. Equal apportionment of the error EW and NS (see 2.2.2.1.2) thus reduces each of the above values by a factor of almost $\sqrt{2}$, to yield the final values.

(The plausible error might be further decreased by another factor of ten because the most likely candidates for the unseen secondary are low-mass main-sequence stars, which would be not 3 but at least 5.5 magnitudes fainter than IM Peg.)

EW – 1 σ	0.001 mas/yr
NS – 1 σ	0.001 mas/yr

3.2.2.5 Flares and other transient events

Flares can cause parts of the disk of a star to brighten in a matter of minutes to twice or more their previous surface brightness. The enhancement generally fades away over a few hours, rarely lasting even a day. Several large flares have been detected on RS CVn stars over the years (*e.g.*, Henry and Newsom 1996). Flares have not been detected on IM Peg in multiband photometry, in spite observations on more than 300 nights by Henry and Newsom with sensitivity better than 0.1 mag brightening in U band. (A flare with 0.1 mag brightening in U band would have significantly less than 0.1 mag brightening in the longer wavelength GP-B pass band.) Nevertheless, these observations show only that, in at least some years, detectable flares are present less than 1% of the time on IM Peg.

The GP-B data analysis can flag any telescope data for which the total detector current is significantly larger than normal. For example, a cutoff corresponding to a 10% increase could be used. Thus, the worst-case undetected flare that could influence the GP-B pointing is one which contributes from a small region near the limb of the star an extra photon flux equal to 10% of the pre-flare output of the star. Since the stellar radius subtends 0.7 mas, such a flare would instantaneously shift the optical centroid of the star, and hence the guide point, by ~0.06 mas. This shift is comparable in size to the orbit-averaged shift in the centroid of IM Peg due to spots, as computed by (Berdyugina, 2002). However, each flare will likely last only hours, and thus cause less than one hundredth the offset to mean proper motion during the GP-B mission caused by a large star spot that lasts for several months. The plausible error is thus entirely negligible.

EW – 1 σ	0.00 mas/yr
NS – 1 σ	0.00 mas/yr

REFERENCES

Armstrong, J. T., et al., The Navy Prototype Optical Interferometer, Astrophys. J., 496, 550, 1998.

Bartel, N., http://aries.phys.yorku.ca/~bartel/GPBresults.html, 2002.

Berdyugina S.V., A.V. Berdyugin, I. Ilyin, and I. Tuominen, The long-period RS CVn binary IM Pegasi; I. Orbital and Stellar Parameters, Astron. Astrophys. , 1999.

Berdyugina S.V., A.V. Berdyugin, I. Ilyin, and I. Tuominen, The long-period RS CVn binary IM Pegasi; II. First surface images, Astron. Astrophys. , 360, 272, 2000.

Berdyugina S.V., ETH Zurich, private comm., 2002.

Bernier, R., T. Acworth, J.P. Turneaure, D. DeBra, Flight Telescope/Window System Verification. GP-B doc. S0570, Revision -, 2001.

Chandler, J. , M.I. Ratner, A Monte Carlo Study of GP-B Errors Due to a Third Body in the IM Peg (HR 8703) System, GP-B doc. S0940, Revision -, 2003.

Drilling, A.S., and A.U. Landolt, Normal Stars, in Allen's Astrophysical Quantities, A. Cox, ed. (AIP Press, New York), p.381, 2000

Duquennoy A., and M. Mayor, Multiplicity among solar-type stars in the solar neighbourhood; II. Distribution of the orbital elements in an unbiased sample, Astron. Astrophys. 248, 485, 1991

Duquennoy, A., & Mayor, M. 1991, Astron. Astrophys., 248, 485, "Multiplicity among solar-type stars in the solar neighborhood. II - Distribution of the orbital elements in an unbiased sample"

ESA, The Hipparcos and Tycho Catalogues, ESA SP-1200, 1997.

Everett, M. E., Howell, S. B., van Belle, G. T., & Ciardi, D. R., 2002, PASP, 114, 656, "Stellar variability in a survey of field stars"

Gilmore, G. F., and M. Zeilik, Star Populations and the Solar Neighborhood, in Allen's Astrophysical Quantities, A. Cox, ed. (AIP Press, New York), p.471, 2000

Goebel, J.H., Response to GP-B Science Committee Questions: Response to Question III.1, GP-B doc. S0490, Revision B, 2001.

Hall, D. S. 2000, in Allen's Astrophysical Quantities, 4th edition, A. N. Cox, ed. (Springer, New York), p. 398, "Variable stars"

Henry, G. W., and M. S. Newsom, A Search for Optical Flares in Chromospherically Active Stars, PASP, 108, 242, 1996.

Henry, G., Tennessee State University, private comm., 2002.

Hoffleit, D., & Jaschek, C. 1982, The Bright Star Catalog, 4th edition, (Yale U. Observatory, New Haven)

Hoffmeister, C., Richter, G., & Wenzel, W. 1985, Variable Stars, S. Dunlap translator, (Springer, Berlin)

Huff, L., K. Bower. GP-B Telescope "Telescope Field of View Test Summary". GP-B doc. S0364, Revision -, 1999.

Humphreys, R.M., R. Landau, F.D. Ghigo, W. Zumach, A.E. LaBonte, BVR Photoelectric Sequences for Selected Fields in the Palomar Sky Survey and the Magnitude-Diameter Relation, Astron. J., 102(1), 395-427, 1991.

Johnson, H. L. 1965, Astrophys. J., 141, 923, "Interstellar extinction in the Galaxy"

Johnson, H. L., Astronomical Measurements in the Infrared, Ann. Rev. Astron. Astrophys., 4, 193, 1966.

Keiser, G.M., M.I. Heifetz, A.S. Silbergleit, New Error Tree, GP-B doc. S0292, Revision C, 1998.

Krautter, J. 1996, in Light Curves of Variable Stars, C. Sterken and C. Jaschek, eds. (Cambridge U. P., Cambridge), p 53-59, "Flare Stars"

Lebach, D. E., et al., Milliarcsecond change of IM Pegasi radio position in 1 hour coincident with sharp rise in flux density, Astrophys. J, 517, L43, 1999.

Mathis, J.S., 2000, in Allen's Astrophysical Quantities, 4th edition, A. N. Cox, ed. (Springer, New York), p523-544, "Circumstellar and interstellar material"

Mayor, M., & Mazeh, T. 1987, Astron. Astrophys., 171, 157, "The frequency of triple and multiple stellar systems"

Ransom, R.R., N. Bartel, M.F. Bietenholz, M.I. Ratner, D.E. Lebach, I.I. Shapiro, J.-F. Lestrade, VLBI imaging and astrometry of the Gravity Probe B guide star HR 8703, in Future Directions in High Resolution Astronomy, J.D. Romney and M.J. Reid, eds., in press, 2003.

Ratner, M.I., J.J. Kolodziejczak, Verification of Knowledge of Guide Star Proper Motion from VLBI Measurements, GP-B doc. S0890, Revision -, 2003.

Shatten, K.H. & J. Orosz, Solar constant secular changes, Solar Phys., 125, 179-184, 1999

Tokovinin, A.A., On the multiplicity of spectroscopic binary stars, Astron. Letters, 23, 834, 1997.

Turneaure, J.P., M.I. Heifetz. Flight Telescope/Window System Analyses of Wavelength Dependent Properties. GP-B doc. S0619, Revision -, 2002.

APPENDICES

Appendix A – Tree-diagrams of error terms. (jjk)

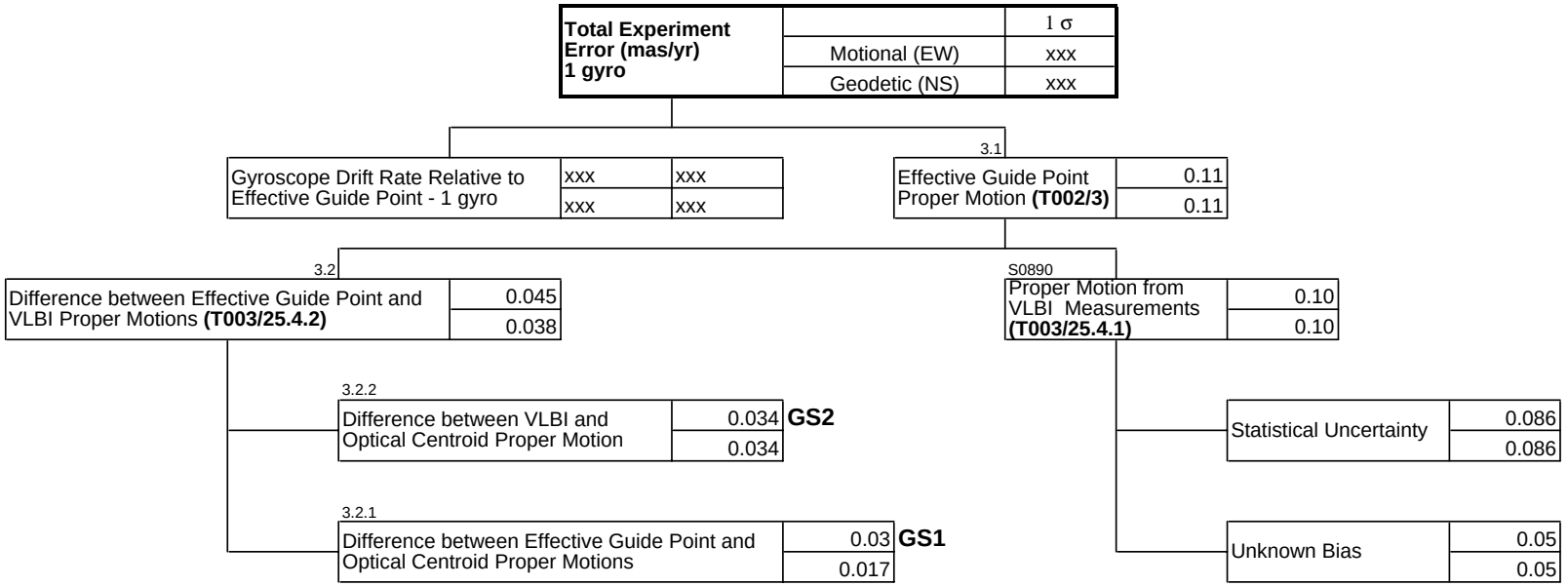

Figure A-1. Top level error tree. EGP proper motion is expanded into two components. The reference "GS1" refers to the error tree show in Figure A-2. The reference "GS2" refers to the error tree shown in Figure A-3. VLBI proper motion is the subject of S0890 (Ratner, 2003). Keiser, *et al.*, (1998) address the GP-B experiment's instrument-related error tree.

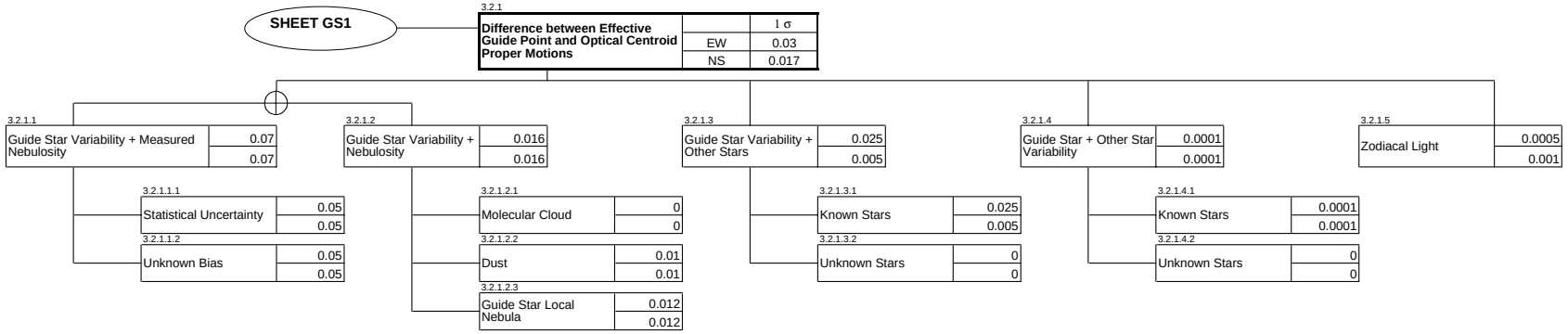

Figure A-2. Error tree components for the difference between effective guide point proper motion and optical centroid proper motion. The encircled "+" sign represents a logical "or" between boxes where only the content of the box with the smaller value is propagated upward.

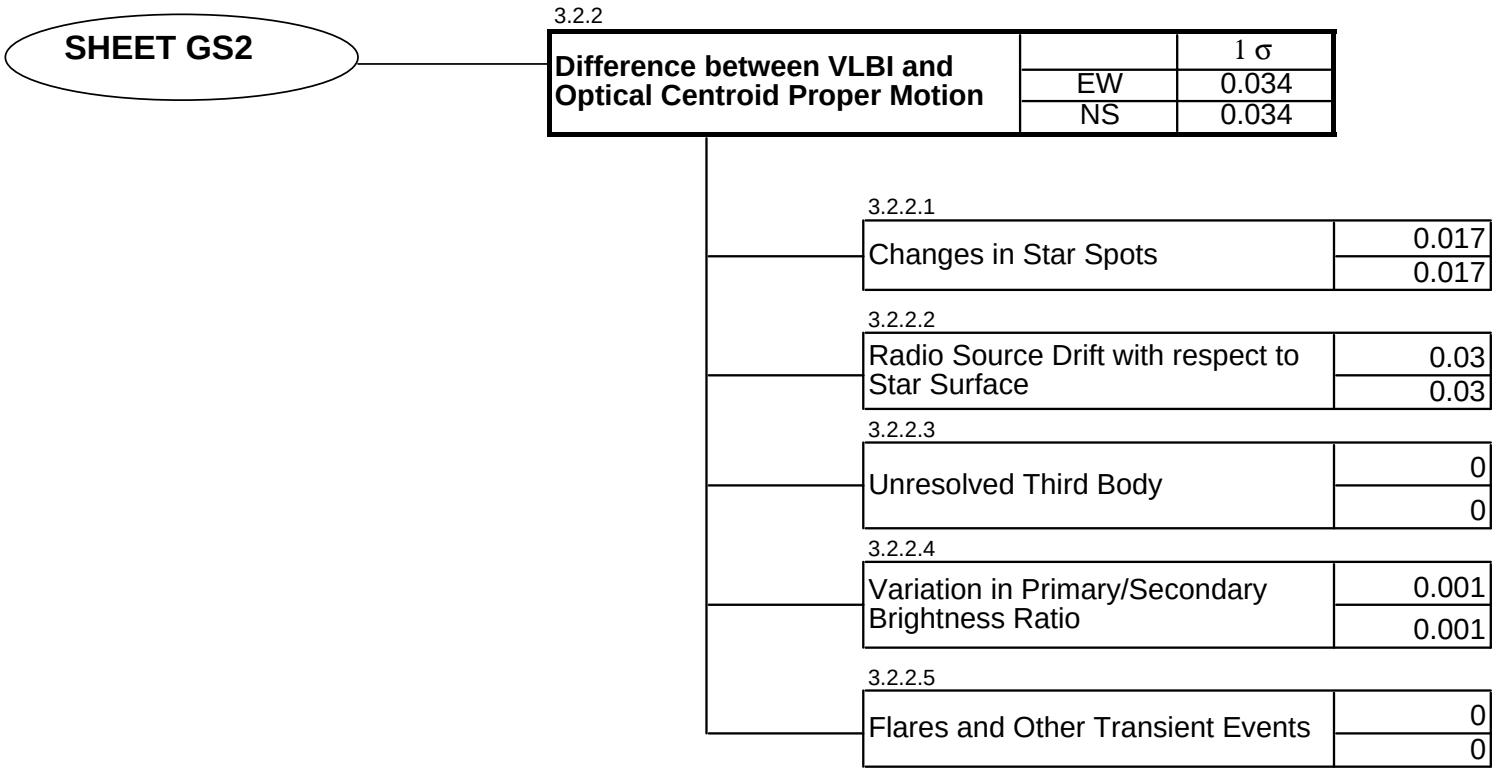

Figure A-3. Error tree components for the difference between VLBI proper motion and optical centroid proper motion.

Appendix B – Guidelines for boxes under Error Tree Item 3.1

1. No box should include errors resulting from uncertainty in GP-B instrumental characteristics. They include uncertainties in astrometric, photometric or other astrophysical quantities only.

2. All boxes contain only the net uncertainty in quantities after roll-averaging.

3. All boxes contain only the net uncertainty in quantities after averaging over a guide star orbit.

4. Plausible-case values are included for each box. These are defined in Appendix C.

5. Worst-case values are estimated in appendices to identify low-probability unknowns, and thereby identify those terms requiring mitigation strategies.

6. The relativistic drift rate is a vector quantity defined in 2 dimensions with an East-West (EW) component and a North-South (NS) component. Both of these quantities are included for each box.

7. When the direction of a vector quantity is known the errors will be apportioned to the EW and NS components with proper accounting for uncertainty in both magnitude and direction.

8. When the direction of a vector quantity is unknown the errors will be apportioned as if the direction is 45° for the plausible case, and treated as if the full magnitude of the error is in each component direction for the worst case.

9. If the box includes effects which depend on guide star variability, then assume a plausible secular change of 5% and a worst-case secular change of 15% based on Appendix D.

Appendix C – Glossary

Astrometric pointing bias – the difference between the effective guide point and the guide star optical centroid.

Detected photon flux imbalance -- the difference between the number of photons from sources other than the guide star which are detected per unit time from the two regions of the sky image on opposite sides of a line through the guide star which bisects the science telescope (ST) field of view (FOV) at some roll angle.

Effective guide point -- the position on the sky where the detected photon flux imbalance is zero for both axes of the ST detector system. This position may be computed either instantaneously or time-averaged over suitable periods, e.g. spacecraft roll, guide star orbit, etc. *Guide Star* – the (binary) star IM Pegasi (=HR 8703), including its primary (i.e., brightest) stellar component and the unresolved and unidentified secondary, which orbit each other with the spectroscopically determined orbital period of 24.649 days. If any additional gravitationally bound components exist which are not fully resolved from the primary by the science telescope, then these, too, would be considered part of the guide star.

Guide Star Optical Centroid – the time dependent celestial position of the centroid of photons from the guide star detected by the GP-B science telescope.

Gyroscope Drift Rate – the rate of change in the spin axis direction of any GP-B gyroscope with respect to the effective guide point.

ICRF -- the International Celestial Reference Frame, the reference frame embodied in an evolving catalog of positions for a subset of the radio sources included in the ICRS.

ICRS – the International Celestial Reference System. A celestial coordinate system based on the set of positions of the radio emission of a set of distant radio galaxies and quasars. Reference frames in this system, e.g., the ICRF, are designed to approximate an inertial reference frame.

Inertial reference frame -- A reference frame which is fixed, in orientation and origin, with respect to the spin axis of any undisturbed gyroscope.

Low-probability potential unknowns – sources of uncertainty whose likelihood of occuring or existing is significantly less than 10%, but greater than or on the order of 0.1%, which, if unmitigated, would result in a worst-case error which is significantly (>33%) larger than three times the plausible case error.

Plausible Case Error – the largest error magnitude that will be reached or exceeded with probability at least 31.8%. Since this probability is the probability that the magnitude of an error with a Gaussian probability distribution will be larger than the standard deviation of its distribution, the plausible case error is just the usual "1-sigma" value if the error distribution is Gaussian.

Proper Motion – the rate of change in the solar-system barycentric celestial coordinates (right ascension and declination referenced to a fixed epoch, e.g., J2000) of a celestial object, exclusive of any known periodic orbital motion. (The procedures used to transform position coordinates measured on the rotating earth and on spacecraft to these J2000 coordinates are specified so as to yield an approximately inertial coordinate system.)

Statistical Uncertainty – the contributions to experimental error resulting from noiselike errors in measured quantities.

Unknown Bias - the contributions to experimental error due to all causes other than those included in the statistical uncertainty.

Worst Case Error – the largest error magnitude that will be reached or exceeded with probability at least 0.54%. Since this probability is the probability that the magnitude of an error with a Gaussian probability distribution will be larger than the standard deviation of its distribution, the plausible case error is just the usual "3-sigma" value if the error distribution is Gaussian.

Appendix D – Proper motion of the effective guide point resulting from guide star variability combined with other sources in the GP-B telescope field of view.(jjk)

The effective guide point will likely have a secular component of proper motion arising from other resolved stars in the field of view because:

1. An instantaneous astrometric pointing bias arises as a result of the presence of an additional star.
2. The pointing bias is in the inertial frame, not the vehicle frame, and therefore does not roll-average to zero.
3. A secular change in the intensity of either the guide star or the other star will lead to secular apparent proper motion.

If not taken into account, this effect of other resolved stars will result in a gyro drift rate error. The magnitude of the effect depends on the brightness, color, and location of the other star. The direction depends on the location and may depend on telescope aperture stop alignment. The effect of multiple other stars is the vector sum of the effect of each individual one. These effects are described in detail below.

Pointing Bias

GP-B uses a control loop to maintain fine pointing where control effort is supplied by two sets of orthogonally directed Helium thrusters. When the control loop is operating in a mode where the telescope signal is used as a primary sensor (guide-star-valid or GSV), then the control system endeavors to nullify the signals arriving from opposite sides of each of two nearly orthogonal roof prisms at the telescope focus. The point where these two signals are precisely balanced is, by definition, the effective guide point. There are two independent control loops for the two orthogonal axes of the space vehicle in the plane to which the pointing direction is normal. We will call these the *x* and *y* axes.

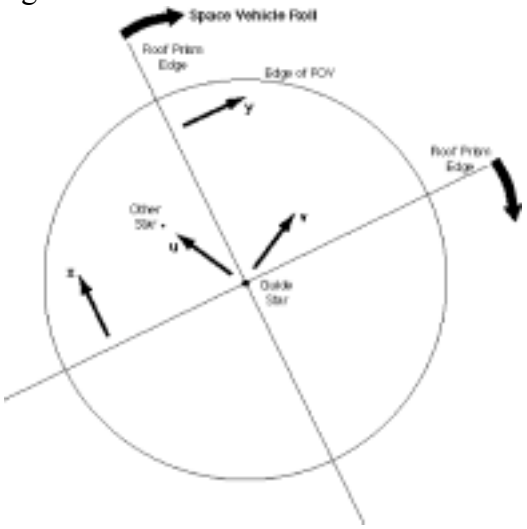

Figure D-1. GP-B telescope conceptual elements referenced in text.

If we consider a single star other than the guide star in the telescope field-of-view, as shown in fig. D-1, then we can define another set of axes *u* and *v*, where **u** is a unit vector in the direction from the guide star to the other star and **v** is perpendicular in the left-hand sense, *i.e*., in the same sense as the right ascension-declination system on the sky. As the space vehicle rolls, the *x* and *y* axes rotate in the *u*-*v* coordinate system, which is inertially fixed (except for the small effects of aberration, proper motion, etc.). When the space vehicle roll orientation is such that the *u* axis has a component in the +*y* direction, the pointing direction will be biased by an amount δ in the +*y* direction as a result of the control system's nulling effort. The value of δ depends on the derivative of the normalized telescope pointing signal with respect to pointing angle, $dS/d\theta$, as defined in (Bernier, 2001) and (Turneaure, 2002). The value of δ also depends on the ratio of the telescope signal current, i_{gs}, due to photons from the guide star to the telescope signal current, $i_{os,}$ due to photons from the other star. The bias results from the fact that the location on the sky corresponding to a null normalized telescope pointing signal (the effective guide point) differs when the other star is present in the telescope field of view relative to the case when it is not present. The two cases are illustrated in an exaggerated way in figure D-2. The change in position is enough to balance the additional light from the other star, so that, for both the *x*- and the *y*-axis detector pairs, the opposing detectors each put out equal currents $(i_{gs} + i_{os})/2$. (Here, for simplicity, we ignore the fact that there are actually two redundant pairs on each axis; in practice, the redundant current signals could be averaged before they are used. Moreover, the ratio between i_{os} and i_{gs} will be different for each detector pair due to color corrections, as discussed below.) If $i_{os} << i_{gs}$ and if the two stars are fully resolved (in contrast to the case of an unresolved star, discussed below), the change in position is

$$\delta = \frac{i_{os}/i_{gs}}{dS/d\theta} \quad . \qquad (1)$$

(Turneaure, 2002) gives a worst case value for $dS/d\theta$ of 0.44 arcsec^{-1}. Arguments in (Bernier,2001) indicate that the most plausible value for $dS/d\theta$ is not more than 10% greater, so we will use this worst case value for all calculations. It follows that a displacement of 1 mas corresponds to $i_{os}/i_{gs} = 0.00044$, or an 8.39 magnitude difference, for a star with the same spectral energy distribution as the guide star.

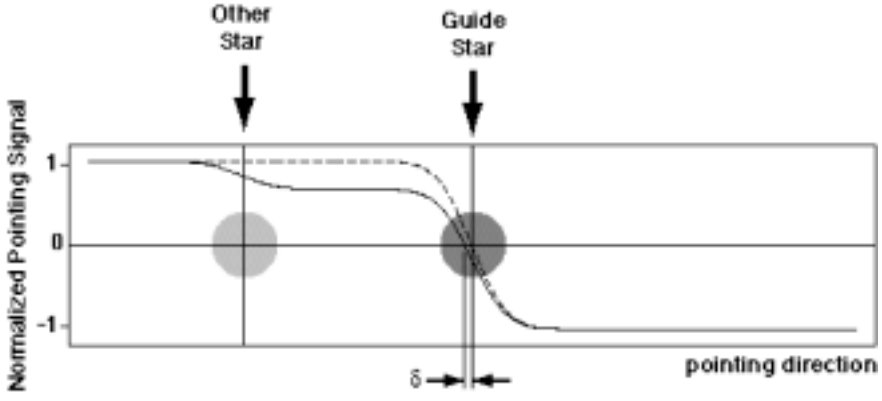

Figure D-2. Pointing bias, δ, resulting from another star in the field of view (schematic). The dashed line indicates the normalized pointing signal for either axis, as a function of

the pointing along that axis, in the presence of the guide star alone. The solid line indicates the normalized pointing signal in the presence of the both stars.

Roll-Averaging

It is the secular component of a time-dependent guiding error that will map directly into errors in the GP-B relativity results. Moreover, to the extent that any error is removed by roll averaging, it will not affect those results. Therefore, we next consider the roll-averaged value of the pointing bias due to the other star. (Note that the maximum instantaneous pointing bias due to known stars will be shown to lie well within the ~100 mas linear range of the telescope readout signal. Thus the net effect of multiple sources of background light in the telescope field of view can be computed as the vector sum of their individual effects.)

The results of the GP-B experiment are not significantly sensitive to the roll-angle-dependence of the pointing bias as long as :

1. the dependence is small, so that the attitude control continues to operate in the linear range of the telescope, ~100 mas, during an entire roll period.
2. the roll-averaged bias does not drift by an amount which is significant compared with the experimental error over the duration of the experiment.

The roll-averaged bias due to the other star can be computed in the essentially inertial *u*-*v* coordinate system from the predicted time-dependent displacements δ_x and δ_y along the rotating *x* and *y* axes. The signs of δ_x and δ_y are always the same as the signs of the dot products of **u** with the **x** and **y** unit vectors, respectively. The roll-averaged effect of the other star is the time average of the vector sum of the **u** and **v** components of this displacement. For simplicity, we make the approximation that the edges of the two roof prisms are exactly orthogonal and aligned with the *x* and *y* axes, even though these edges are actually orthogonal only to within some tolerance. (The actual angle between them may need to be explicitly taken into account in a more exact model of the bias, if one is needed for an adequate model of the relativity signals.) For now, we also ignore the finite size of the image of the second star. In this approximation, the **u** component of the bias is given by

$$\bar{\delta}_u = \frac{\omega_r}{2\pi} \int_{roll} \left(|\delta_x \cos\omega_r t| + |\delta_y \sin\omega_r t| \right) dt = \frac{4\delta}{\pi} \qquad (2)$$

and the **v** component is given by

$$\bar{\delta}_v = \frac{\omega_r}{2\pi} \int_{roll} \left(\delta_x \frac{\sin\omega_r t \cos\omega_r t}{|\cos\omega_r t|} - \delta_y \frac{\cos\omega_r t \sin\omega_r t}{|\sin\omega_r t|} \right) dt = 0 \ . \quad (3)$$

In these integrals we have chosen the origin of t so that $\omega_r t$ is the angle between the *x* and *u* axes and thus the time-dependent *x* component of the bias is $\delta \times$ signum(cos $\omega_r t$), and similarly for *y*. It follows that the roll-averaged effect is a displacement $(4/\pi)\delta$ in the direction **u**, where δ is given by eq. 1. For the more general case, where $\delta_x \neq \delta_y$, the simple average $\delta \equiv (\delta_x + \delta_y)/2$ can be used. Figure D-3 shows this roll dependence for the simple case $\delta_x = \delta_y \equiv \delta$. The pointing direction then traces a 90 degree arc of a circle with radius $\sqrt{2}\delta$, at a frequency of 4 times per roll period, as shown in figure D-3(c).

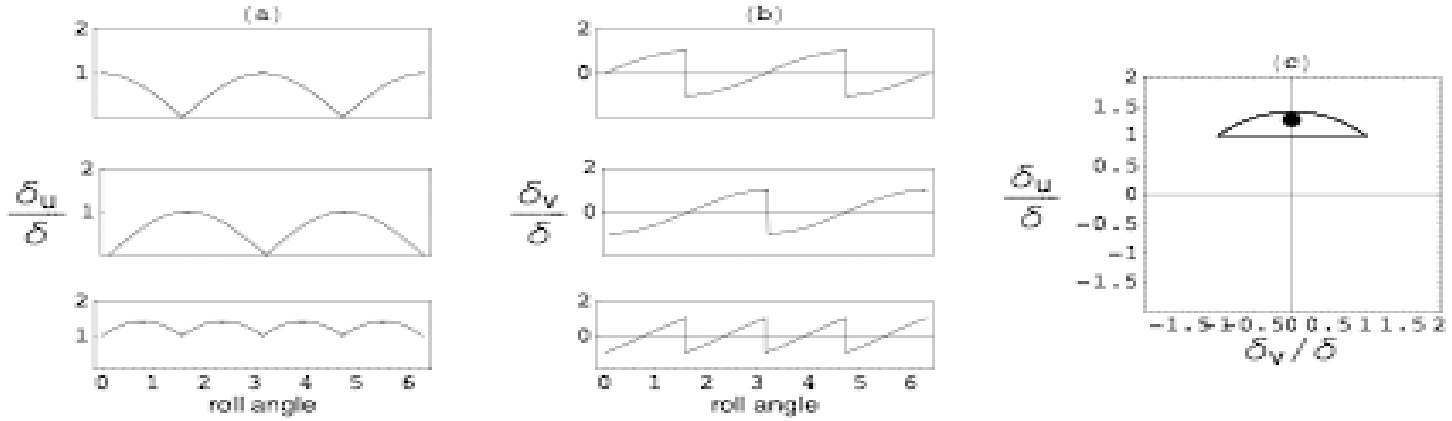

Figure D-3 . Roll-angle dependence of pointing bias. (a) The upper panel is the *x* contribution to the ***u*** component, the middle is the *y* contribution to the ***u*** component, and the bottom is the sum. (b) The same quantities for the ***v*** component. (c) Trace of the guide-point offset in the *u*-*v* plane over each quarter roll period**.** The (horizontal) return sweep occurs relatively quickly, as the image of the second star crosses one of the roof prisms in the focal plane**.** The heavy black dot indicates the roll-averaged bias, which in our approximation is the "centroid" of the circular arc.

Vignetting

The telescope response to objects near the edge of its field of view is affected by the following factors:

1. The telescope's field-of-view is vignetted at its edge as a result of the aperture stop which is located at a focal depth where the defocused PSF has a diameter of approximately 25 arcsec. In addition, azimuthal variations in the PSF give an azimuthal dependence to the width of the vignetted region.
2. The telescope optical axis (defined as the body-fixed instantaneous pointing direction assuming a single ideal point source in the field of view) is displaced from the exact center of the nearly circular field of view. This also causes the amount of vignetting associated with a star at a given radius from the guide star to vary with roll angle.

The result of any vignetting is to reduce the signal from the other star, and therefore its effect on the pointing. However, uncertainties in the two factors listed above would cause a correction calculated for a known star in the vignetted region to have a larger uncertainty than a similar star in the unvignetted region.

If the vignetting function is $V(r,\theta)$, then the **u** component of the roll-averaged displacement due to a vignetted star at radius r is given by

$$\bar{\delta}_u = \frac{\omega_r}{2\pi} \int_{roll} V(r,\theta(t))\left(\left|\delta_x \cos\omega_r t\right| + \left|\delta_y \sin\omega_r t\right|\right)dt \qquad (4)$$

and the **v** component is given by

$$\bar{\delta}_v = \frac{\omega_r}{2\pi} \int_{roll} V(r,\theta(t))(\delta_x \frac{\sin\omega_r t\cos\omega_r t}{\left|\cos\omega_r t\right|} - \delta_y \frac{\cos\omega_r t\sin\omega_r t}{\left|\sin\omega_r t\right|})dt\,. \qquad (5)$$

Based on (Huff, 1999), the alignment errors for the x and y axes are +4.5 and +2.9 arcsec, respectively, with uncertainty of ±1 arcsec. Based on ref. 13, the vignetting function may be reasonably approximated by the following function going from 1 at 45 arcsec to 0 at 70 arcsec:

$$V(r,\theta) = 2.8 - \frac{\sqrt{\left(r\cos\theta - x_0\right)^2 + \left(r\sin\theta - y_0\right)^2}}{25}\,. \qquad (6)$$

We used a simulation of 5000 random alignment positions with an error ±2 arcsec at each of several star radii to derive the plausible bias due to vignetted stars shown in figure D-4. Fig. D-4 shows only the **u**-component of bias because the **v**-component was at most a negligible, 0.003δ.

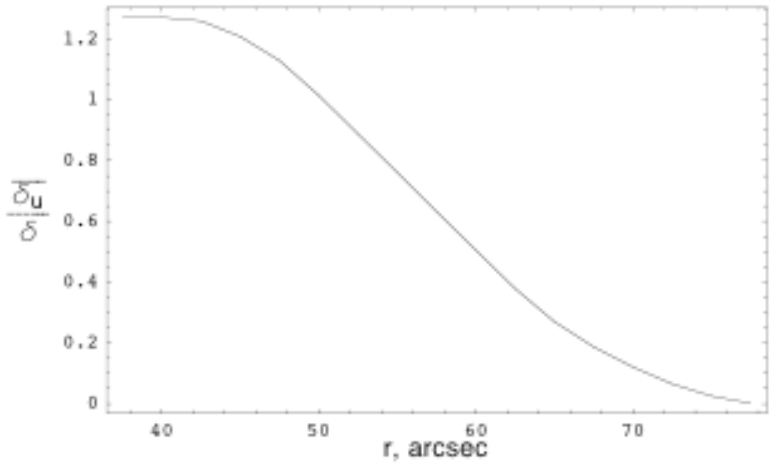

Figure D-4. Roll-averaged vignetting factor across the edge of the field of view

Brightness Variation

If the roll-averaged bias discussed above were constant, then an additional star in the field of view would have no effect on GP-B's results. However, the guide star is, in fact, an RS CVn type binary star, and exhibits secular changes in brightness on time scales of months to years, as well as nearly periodic changes. The periodic variability does not affect the result, since the photometric period is known to be ~24.4 days, and the experimental results are not biased by variations near this period. It may be possible to place experimental limits on the effect of other stars on the proper motion by analyzing the signal in the GP-B data near the binary period. The errors associated with such an analysis are not included in this version of the error tree.

Fig. D-5 (a) shows the variation in the guide star intensity over a period of 14.4 yrs from 1987 to 2002 (ref. 16). We performed the following steps to obtain estimates of the plausible and worst case annual linear slopes in the HR 8703 intensity.

1. Divide the data into observational episodes where no pair of consecutive observations within an episode is separated by more than 22 days, and the time between the end of one episode and the beginning of the next is at least 30 days.
2. Determine the maximum and minimum of data for each episode and the time midpoint between the maximum value and the minimum value
3. Create linear interpolation functions for the maximum points vs. time and the minimum points vs. time as shown in figure D-5 (a).
4. Construct a smoothed curve representing the mean of the maximum and minimum interpolation functions. The smoothing is done by filtering to include only Fourier coefficients at frequencies below 1.5/year.
5. Create a table of "mean" values vs. time from the smoothed curve and partition the table into subsets of 1 year duration and starting at 3 month increments.
6. Perform a linear fit on each subset to determine the slope in magnitudes per year, and bin the absolute values of the slope from each of four sets of independent values to create four distributions of slopes. The integrals of these distributions

are the cumulative distribution functions (CDF) shown in figure D-5 (b). The plausible errors due to the slope are computed for the absolute value of the slope that was exceeded with 30% probability in these four distributions as discussed below.

7. To estimate the worst case, we synthesized 5000 years worth of data using the following procedure:
    a. Obtain the Fourier transform of table of "mean" values vs. time;
    b. Create a similar Fourier transform using frequencies lower than 1.5/year by randomizing the Fourier amplitudes by a Gaussian with s giving a factor of 50%, and randomizing the phases over a uniform distribution;
    c. Take the inverse Fourier transform of this distribution to probe how plausible variations in the amplitudes and phases of the Fourier components of the photometric variations of HR 8703 can combine to give a worst case slope;
    d. Generating 5000 years worth of data in this way produces the CDF shown in figure D-5 (c).

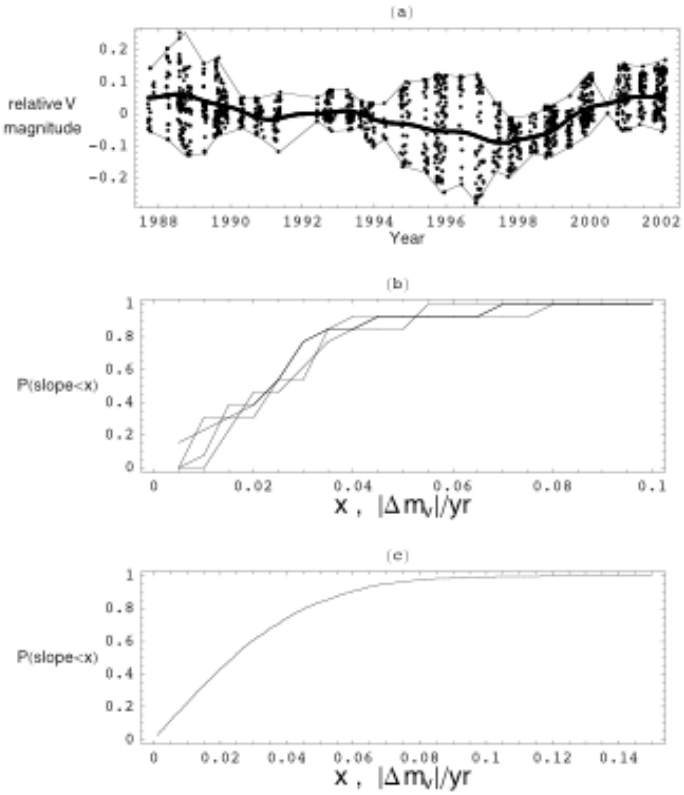

Figure D-5. Statistical analysis of the variation in flux from HR 8703. (a) Measured data with secular trend. (b) CDF of the absolute change in visual magnitude per year, x, from measured data. The four curves are results of partitioning the measured data starting from four different starting points, each separated by 3 months. (c) CDF of the absolute change in visual magnitude per year, x, from 5000 yrs of synthesized data, as described in the text.

The plausible case obtained by this procedure is 5% / yr consistent with both figures D-5 (b) and (c). The worst case obtained from figure D-5 (c) at the 99.8% probability level is 12% / yr. We assume 15% /yr for the worst case to make some allowance for the limited span of time on which this simulation is based.

Color Correction

The displacement resulting from another star in the field of view depends on the star's color. The color can be accounted for in the factor i_{os}/i_{gs} using the following formula based on BVRI magnitudes and the characteristics of the GP-B telescope and the guide star. (If a color correction is calculated as part of the science data analysis procedure, some account may need to be taken of the U band and ~1 micron regions of the spectrum, as well. However, for simplicity, these regions of relatively low expected response of the GP-B detectors are not considered here.) For each detector pair $n = 1,4$

$$\frac{i_{os}}{i_{gs}} = \frac{\sum_{j=VBRI} \lambda_j \Delta\lambda_j T_{winj} T_{telnj} \varepsilon_{PDj} f_{0j} 10^{\frac{(-m_j)_{os}}{2.5}}}{\sum_{j=VBRI} \lambda_j \Delta\lambda_j T_{winj} T_{telnj} \varepsilon_{PDj} f_{0j} 10^{\frac{(-m_j)_{gs}}{2.5}}} = \sum_{j=VBRI} k_j 10^{\frac{(-m_j)_{os}}{2.5}}. \qquad (7)$$

Table 1 summarizes the values from (Turneaure, 2002) and (Drilling, 2000) for parameters in this formula for each of the four detector pairs. Table 2 relates various color corrections, allowing all the VBRI magnitudes to be determined from any two of the V, B, R, I, O, or E magnitudes, based on the relations in (Drilling, 2000) and (Humphreys, 1991). E and O magnitudes refer to the effective wavelength bands of the red and blue plates used in the Palomar Sky Survey, and are related to R and B using (Humphreys, 1991).

j	wavelength band	B	V	R	I
λ	central wavelength, μm	0.44	0.55	0.7	0.9
$\Delta\lambda$	width of band, μm	0.10	0.13	0.17	0.2
$\log_{10} f_0$	Log of flux in W cm^{-2} μm^{-1} at 0 magnitude	-11.18	-11.42	-11.76	-12.08
T_{win}	window transmission	0.63	0.73	0.80	0.78
T_{tel1}	telescope transmission, detector pair 1	0.038	0.037	0.023	0.025
T_{tel2}	telescope transmission, detector pair 2	0.047	0.047	0.041	0.04
T_{tel3}	telescope transmission, detector pair 3	0.031	0.036	0.028	0.023
T_{tel4}	telescope transmission, detector pair 4	0.056	0.049	0.034	0.043
ε_{PD}	detector quantum efficiency	0.5	0.68	0.73	0.75
m_{gs}	HR 8703 magnitude	7.15	6.01	5.10	4.54
k_1	weighting factor, detector pair 1	37.8	54.2	30.2	23.8
k_2	weighting factor, detector pair 2	30.0	44.2	34.5	24.4
k_3	weighting factor, detector pair 3	30.3	51.8	36.1	21.5
k_4	weighting factor, detector pair 4	36.2	46.6	29.0	26.6

Table D-1. Properties required for color corrected i_{os}/i_{gs}.

Normal star type	B – V	V-R	R-I	O-B	E-R	O-E	B-R
A0	0	0	0	0	0	0	0
F0	0.27	0.30	0.17	0	0.05	0.52	0.57
G0	0.58	0.52	0.41	0	0.05	1.05	1.10
K0	0.89	0.74	0.66	0.05	0.10	1.58	1.63
M0	1.45	1.10	1.10	0.10	0.40	2.25	2.55

Table D-2. Color relationships for normal, stars for BVRI and Palomar Plate O and E. Application of eq. 7 results in fig D-6. Fig. D-6 (a) shows how the pointing bias depends on star magnitude for a A0-type normal star. Figs. D-6 (b) and (c) show how the pointing bias depends on color indices, (B – V) and O-E.

Summary

Figure D-7 shows the V magnitude required to produce a proper motion in the effective guide point of 0.1 mas/yr as a function of color index B-V, under the plausible assumption of a 5% per year change in the guide star flux.

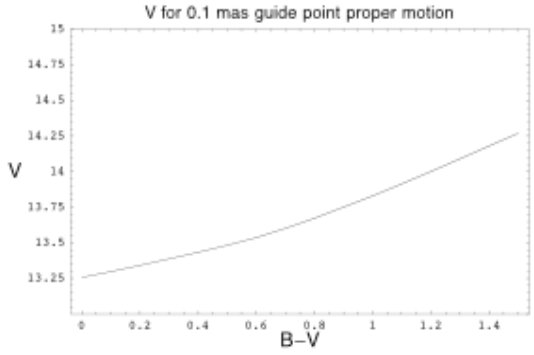

Figure D-7. V magnitude required to produce an effective guide point proper motion of 0.1 mas/yr, assuming a plausible flux variation of 5% per year

Additional Sources

The displacements from multiple sources in the unvignetted region of the field of view are vector-summed. The effect in the vignetted region has a random component resulting from the uncertainty in the alignment and PSF, but this component is small. For simplicity, erring on the conservative side, we also vector-sum these error contributions.

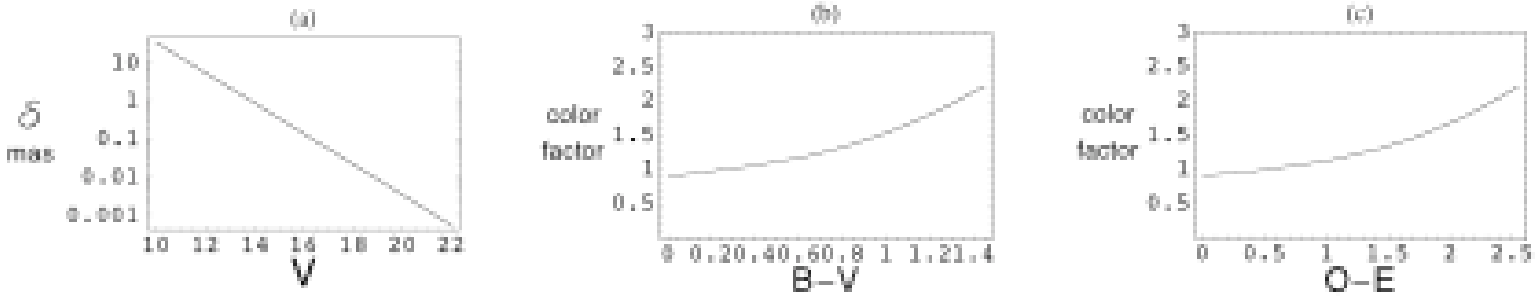

Figure D-6. Effects of spectral type on pointing bias. (a) Pointing bias for an A0 type normal star. (b) Scale factor required to account for the dependence of pointing bias on color index, B-V. (c) Scale factor required to account for the dependence of pointing bias on color index O-E.

Nebulosity

In order to consider the effects of nebulosity, we integrate the field of view with the vignetting function shown in figure D-4. This integral gives 10732 arcsec^2. A spatial variation in nebulosity could result in an inertially fixed pointing bias, which in combination with guide star variation, could alter the proper motion in the effective guide point. Based on considerations above, we assume that an instantaneous pointing bias of 1 mas corresponds to $i_{os}/i_{gs} = 0.00044$. A diffuse source filling half the telescope field of view with surface brightness that produces a current per square arcsecond averaging $0.00044*2/10732\ i_{gs} = 8.2\text{x}10^{-8}\ i_{gs}$ arcsec^{-2} could introduce this level of instantaneous pointing bias.

After roll-averaging, the effect of a diffuse source is smaller than that of a point source. On the other hand, a linear gradient contributes a scaling factor of 1, rather than $4/\pi$, and a step function contributes a factor of $8/\pi^2$. We choose a roll-averaging factor of 1 to conservatively estimate the effects of nebulosity. In Table 3, we give the approximate minimum mean surface brightness of nebulosity required to alter the proper motion of the guide point by 0.1 mas/yr for our plausible and worst cases of 5%/yr and 15%/yr, respectively, of the secular trend in guide star brightness.

Guide star variation	Mean nebulous contribution	Equivalent stellar magnitude
5%/yr	$1.63\text{x}10^{-7}$ arcsec^{-2}	22.9 arcsec^{-2}
15%/yr	$5.46\text{x}10^{-8}$ arcsec^{-2}	24.1 arcsec^{-2}

Table D-3. Spatially averaged nebulosity imbalance to produce a 0.1 mas/yr proper motion component.

Unresolved star **(< ~2 arcsec from guide star)**

For the case of a star very close to the guide star, the pointing bias is smaller than the bias due to a fully resolved star of equal brightness, because the PSF of the telescope results in a continuous sharing of light from the additional star on both sides of each roof prism. This sharing increases until the effect of a brightness change becomes negligible when the additional star is exactly coincident with the guide star. At this point, the only effect is the current-weighted average of the two proper motions. In computing Fig. D-8, we use a simple treatment of the PSF as a Gaussian function and we assume that the additional star has zero proper motion and a Vega-like spectrum, i.e., that all its color indices are zero. The magnitude at zero radius is a result of the fact that 0.1mas/yr is ~0.3% of the proper motion of IM Peg. Note, however, that the assumption of zero proper motion is not appropriate if the additional star is a part of the IM Peg system and hence comoving with it. (The relative orbital motion will likely be less than the proper motion of the IM Peg primary, unless its period is less than about 4 yr, corresponding to a separation less than 0.1 arcsec. In that case, the orbital component will not be even approximately constant during the 1 yr duration of the GP-B mission, and so the secular trend in the pointing bias will be reduced to a greater or lesser degree.) Figure D-8 shows

how maximum magnitude for the other star to be significant depends on its separation from the guide star.

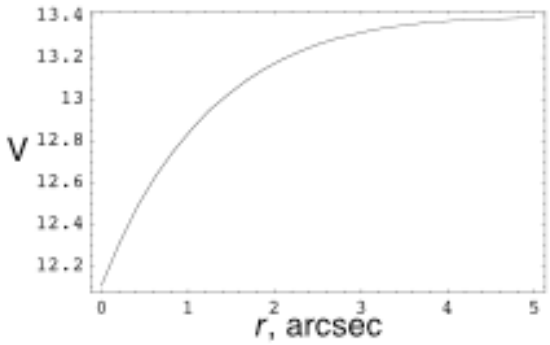

Figure D-8. Required V magnitude for an additional star with B-V = 0 to produce a 0.1 mas/yr proper motion of the effective guide point as a function of separation from the guide star, assuming 5%/yr variation in the guide star luminosity and zero proper motion for the additional star.

Appendix E – Constraints on nebulosity near IM Peg from analysis of HST images. (jjk)

Introduction

This appendix describes an analysis of HST images of IM Peg, which were acquired in 1997. The purpose of the analysis is to establish constraints on a nebulous component in the region of the sky near IM Peg. If such a nebulous component exists and it has a spatial brightness gradient or similar spatial asymmetry with respect to the star, then a change in brightness of IM Peg would produce a drift in the GP-B telescope as discussed in Appendix D.

HST Images

30 images were acquired using the HST WFPC2 instrument (PI: Shapiro, 1997), 15 at each of 2 roll angles, at using various filters and exposure times. In order to decide which images are useful for constraining nebulosity it is important to note that low level signals on the WFPC2 CCDs are subject to random uncorrected bias jumps of order 0.1 DN. If a bias jump of this order occurred at the middle of a WF chip, it would result in a nebulosity gradient bias of .11 (DN/pixel)/arcmin. This bias is a measure of the limit of nebulosity gradient sensitivity of the WF chips resulting from this systematic error. The table below lists the exposures taken and the conversion of .11 (DN/pixel)/arcmin into magnitudes /arcsec^2/arcmin for each exposure.

ID	filter	exposure time (sec)	zeropoint (mag)	gradient sensitivity (mag/sq.arcsec/arcmin)
301,601	F502N	0.50	17.23	13.87
302,602	F953N	1.00	15.27	12.66
303,603	F1042M	1.00	15.27	12.66
304,604	F1042M	1.00	15.27	12.66
305,605	F255W	100.00	16.30	18.69
306,606	F300W	5.00	18.70	17.84
307,607	F850LP	0.14	19.21	14.46
308,608	F850LP	1.00	19.21	16.60
309,609	**F555W**	**6.00**	**21.81**	**21.14**
30a,60a	F555W	0.16	21.81	17.21
30b,60b	**F450W**	**16.00**	**21.25**	**21.65**
30c,60c	**F814W**	**8.00**	**20.91**	**20.56**
30d,60d	F336W	20.00	18.71	19.35
30e,60e	F336W	0.70	18.71	15.71
30f,60f	F336W	4.00	18.71	17.60

Table E-1. Estimated limits of nebulosity gradient accuracy from HST images due to potential systematic errors resulting from bias variations on WFPC2 WF CCDs.

As discussed in appendix D, variations in bias corresponding to a diffuse gradient in V magnitude of 22.9 /arcsec^2/arcmin are required to produce drifts of 0.1 marcsec/yr. Therefore, only images with sensitivity comparable to this are useful for constraining a potential nebulosity gradient. Only 6 images are sufficiently sensitive as indicated in Table E-1 and these cover the I, V and B bands. These images are highly saturated and render the WFPC2 PC chip useless, because of charge bleeding. The analysis that follows uses data from the WF2, WF3 and WF4 CCDs .

Processing

A custom analysis method was developed for this unique application. The method uses combined data from the WF2, WF3 and WF4 CCDs to produce an estimate of the asymmetry of in the diffuse light incident on these CCDs on opposite sides of a bisecting line passing through the guide star. The asymmetry is determined as a function of the angle on the sky of this bisector and the angle where the asymmetry is a maximum is taken as the plausible value. We define the asymmetry as the properly weighted difference in the average DN/pixel between the two side of the bisector.

The algorithm proceeds as follows:

- Gross cut: Pixels with DN above a specific threshold are excluded to eliminate cosmic rays and point sources.
- Signal/noise cut: Local noise is estimated within a specific radius around each pixel and pixels whose signal/noise exceeds a threshold are excluded to eliminate low level effects of the HST point spread function
- Vicinity cut: Pixels within a specified radius of those pixels eliminated in the previous steps are also eliminated to further eliminate telescope related stray light.
- Remaining data is remapped into polar coordinates (θ,ϕ)
- For each ϕ, asymmetry is calculated first vs. θ, then weighted by a coverage factor proportional to θ then integrated over the available θ range.
- The maximum value for the asymmetry as a function of is obtained for each of the two roll configurations and the smaller of the two is choose as the plausible asymmetry.
- The steps are repeated for all of the sensitive files listed in Table E-1.

The specific analysis is performed with Mathematica (see note below)

Results

The results are summarized in Table E-2, which lists the maximum asymmetry obtained from each color band. This maximum represents a plausible bound on the asymmetry resulting from a nebulous component near IM Peg.

Wavelength band	Max asymmetry DN/pixel	Max asymmetry mag/arcsec^2
I (F814W)	0.018	22.5
V(F555W)	0.023	22.8
B(F450W)	0.048	22.5

Table E-2. Results of HST nebulosity analysis

To calculate the error that an asymmetry of this magnitude would produce we take {B,V,R,I}={22.8, 22.8, 22.6, 22.5}. The choice of 22.8 instead of the limit 22.5 is based on the fact that it would be unphysical to have V-I=0.3 and B-V=-0.3. Interpolation gives the images show that the lower sensitivity is the result significantly higher bias variations.

The calculation follows Appendix D, Table 1. An example is shown below, for the worst case of detector pair 1:

$$\frac{(37.8\times10^{\frac{-22.8}{2.5}}+54.2\times10^{\frac{-22.8}{2.5}}+30.2\times10^{\frac{-22.6}{2.5}}+23.8\times10^{\frac{-22.5}{2.5}})/\,\mathrm{arcsec}^2\times(10732/2)\mathrm{arcsec}^2}{(.00044\,\mathrm{mas}^{-1})}\times 0.05/\mathrm{yr}=0.074\ \text{mas/yr}.$$

The EGP drift limit assuming a 5% per year guide star brightness change is 0.07 mas/yr for this level of nebulosity. This is the plausible limit on the EGP drift due to nebulosity. The worst case assumes 15% guide star brightness change which corresponds to 0.21 mas/yr.

Conclusions

Based on this analysis, the nebulosity near IM Peg in the radial range from 18 arcsec to 100 arcsec shows no evidence of magnitude asymmetry brighter than 22.8 /arcsec^2. Assuming the guide star brightness varies 5%/year, this constrains the error from such a nebulous component to less than 0.07 mas/yr.

Note: The specific Mathematica runs for this analysis are available on the GP-B wing of the MSFC VRC (virtual research center) with file names:sep03nebdatAB.nb (roll 1, B filter), sep03nebdatBB.nb (roll 2, B filter), sep03nebdatAV.nb (roll 1, V filter), sep03nebdatBV.nb (roll 2, V filter), sep03nebdatAI.nb (roll 1, I filter), sep03nebdatBI.nb (roll 2, I filter).

Appendix F – Constraints on nebulosity near IM Peg from (other-than-HST) observations and theoretical considerations. (mir)

Scattering of starlight by circumstellar and interstellar dust is the most plausible non-instrumental source of spatially extended, visible and near-infrared continuum emission that might affect the GP-B science data. Therefore, in this appendix we consider observational constraints on the amount of dust in the GP-B field of view.

Notwithstanding the similarity of the potential effects of nebulosity and light from a background stars, the plausible magnitudes of those effects are not equal for stars and nebulosity contributing the same total GP-B detector current. Although background stars can be significantly variable, there is only a very small probability, far less than 0.01, that a star selected at random would vary during any given year by as much as the typical year-to-year variation of IM Peg. On the other hand, depending upon certain unknown geometrical parameters, if the nebulosity were a reflection of the light of IM Peg, the nebulosity seen from Earth likely varies more than the star itself as seen from Earth.

In this appendix, we discuss:
(1) the galactic environment in the general direction of IM Peg;
(2) how the geometry of scattering by dust determines a scale factor in the maximum contribution that dust can make to the GP-B science signal;
(3) the column density of dust in the direction of IM Peg inferred from all-sky IR maps produced by the IRAS and COBE spacecraft;
(4) scattering by an extended dust structure;
(5) IRAS and IRTF mid-IR photometry of IM Peg, which yields inconclusive hints of dust near or within the IM Peg binary system;
(6) 115 GHz observations of IM Peg, which yield no indication of a molecular cloud in the direction of IM Peg;
(7) IM Peg optical polarization measurements some of which yield ambiguous evidence for dust near or within the IM Peg binary system; and
(8) a non-detection of H-α scattering in long-slit spectra of IM Peg.

(1) The Galactic environment of IM Peg

IM Peg is located in a rather undistinguished part of the Galaxy. It's approximate galactic coordinates are (86°, -37°) in the heliocentric spherical coordinate system whose equator is defined by the mean plane of the disk (and spiral arms) of the Galaxy, and whose origin of longitude is the direction of the Galactic center. Thus, our line of sight to IM Peg is well out of the Galactic plane and the prominent Milky Way of the night sky. IM Peg is not notably close on the sky to any obvious feature of the Galaxy, such as a star

cluster or bright visible nebula. The distance of IM Peg, as determined from our own VLBI and verified to slightly less accuracy by Hipparcos, is 95 ± 1 parsecs (pc). This distance places the star significantly out of the Galactic plane yet still close enough to it that the expected properties of its neighborhood might resemble those for the Galactic plane generally, were it not for known local departures from those means. (The Sun is thought to lie even closer to the Galactic plane, only 20 pc "above" the plane according to Gilmore and Zeilik 2000, in Allen's Astrophysical Quantities, A. Cox, ed., AIP Press, hereafter AQ).

What can we say about the likelihood of nebulosity at a level significant for GP-B? The distribution of gas and dust in the Galaxy is inhomogeneous on all observable scales. Nevertheless, it may be useful to keep in mind certain features of their observed distribution in interstellar space.

The densities of both gas and dust vary from place to place over orders of magnitude even in our part of the Galaxy (within, say, a kiloparsec of the Sun and within 100 pc of the galactic plane). However, in the same spatial region, the ratio of the estimated mass density of dust to that of gas is thought to vary by only a factor of a few. (Apparently, the gas and dust are well mixed and more or less moving together, even as they are intermittently heated by short-lived hot stars and supernovae, either of which can alter the bulk velocity of the gas by several km/sec in volumes extending for many parsecs. Likewise, interstellar gas and dust move together when compressed by self- gravitation or by shock waves arising from the impact of neighboring regions with different bulk velocities.) Relatively dense regions occupy only a few percent or less of the volume of space in our part of the Galaxy (Mathis 2000, in AQ), but such regions account for most of the column density of gas and dust, and hence most of the interstellar scattering and extinction, along any given line of sight with a length of a few hundred parsecs or more. These denser regions are termed "clouds," and they are categorized by their total mass, optical depth, mean temperature, method of detection, etc.

And what can be said about our line of sight to IM Peg? Linsky *et al.* (2000, ApJ, 528, 756) identify the outlines of five disjoint regions on the sky (together filling most of the sky) in which light from all but the closest stars suffer significant absorption within certain narrow spectral lines corresponding to various atoms and ions. (Although the mass of the interstellar gas consists almost entirely of ionized, atomic, or molecular hydrogen and helium, many relatively rare species are more easily detected spectroscopically, depending on the local conditions.) Linsky *et al.* infer that light from any distant source in any one of these regions passes through a single relatively nearby gas cloud, each with mean hydrogen density, n_H, perhaps 0.1 cm^{-3}, and characterized by a narrow range of radial velocity with respect to the Sun. It is the consistency of the radial velocities across tens of degrees of the sky that allows the regions, and hence the clouds, to be identified as extended objects. Conveniently for GP-B, IM Peg does not lie within any of the five identified regions.

Moreover, most of the line of sight between IM Peg and us seems to lie within the so-called Local Bubble, which is a volume of space with far lower than average gas density

($n_H \approx 0.001$ cm^{-3}). (Other, more distant but similar voids in our Galaxy are sometimes called "superbubbles.") The existence of the Local Bubble is most plausibly explained as being a result of a concentration of supernova events having a common origin in the grouping of young stars known as the Scorpius-Centaurus Association, which is now ~150 pc away from us in the direction (320°, +15°) (Linsky *et al.* 2000), and hence ~130° away from IM Peg. The Sun is thought to be embedded in the so-called local interstellar cloud, with density of order $n_H \approx 0.1$ cm^{-3}, but close enough to one edge that the line absorption toward IM Peg is relatively small (e.g., Linsky *et al.* 2000). Although the accuracy of this picture is not yet established, it does suggest that most of the line of site between IM Peg and us has far lower than the average amounts of both gas and hence also of dust.

The biggest potential worry for GP-B presented by this picture is that it suggests that IM Peg lies close to, or within, what is expected to be a relatively sharp edge of the Local Bubble. Sfeir *et al.* (1999, A&A, 346, 785) fit a three-dimensional model of the volume density of atomic sodium to measurements of the total amount of interstellar absorption in the sodium D-line doublet in the spectra of 453 stars within ~300 pc. The angular resolution of this model is about 10°, and on this scale the inferred density typically varies by a few tens of percent. They illustrate their model with cross-sections along several planes, including the plane that contains the Sun and is normal to the direction of the Galactic center, i.e., normal to coordinate (0°, 0°). From this cross-section one can infer the radial distribution of the absorbing gas in the direction (90°, -37°), only 3° from IM Peg, out to ~100 pc from the Sun, and thus approximate the distribution along the line of sight toward IM Peg. In the model, more than 60% of the gas along this line is located more than 85 pc from the Sun, i.e., within 10 pc of IM Peg. The resolution of the model is inadequate to localize the gas more precisely.

If the gas and dust originally contained in the Local Bubble have been pushed to its boundary, the thickness of the resulting high-density region could be quite small. The local cloud is modeled by Linsky *et al.* with an atomic hydrogen density of 0.1 cm^{-3}, but they note that if, as they infer, it is currently colliding with a neighboring cloud, the density at the boundary layer could be far higher, limited only by magnetohydrodynamic (MHD) processes there. Without further analysis, they refer to previously published speculation on the climatic consequences for the Earth if that density were to exceed 1000 cm^{-3} or even 10^6 cm^{-3}. It is our understanding that a similar boundary could plausibly exist near IM Peg, which (as discussed above) is perhaps similarly situated near the edge of the Local Bubble. For reasons discussed below, the scattering geometry allowed by dust close to IM Peg could be unfavorable for GP-B. We have not tried to estimate just how high a density of dust, and hence gas, near IM Peg is required to produce a significant amount of nebulosity in the GP-B field of view. Clearly, the higher that density, the more compressed and hence more thin must be any high-density layer lying near IM Peg if it is going to affect the pointing of GP-B, and therefore the less likely it is that a layer would lie in just the right place. The point we would make now is simply that it is not justified to derive a reassuringly low probability for this occurrence by assuming that IM Peg is randomly located in the Galaxy. To the contrary, even though IM Peg is an evolved system far older than the Local Bubble and hence not

causally related to it, IM Peg is nevertheless observed to lie close to the boundary of the Local Bubble. Consequently it has a higher than average chance of lying in a volume with a high density of gas and dust.

(2) The geometry of scattering by dust

The effect on GP-B of visible light scattering by dust depends not only on the optical properties of the dust but also on its location. The minor degree of sensitivity of GP-B to zodiacal dust (the dust in our solar system concentrated near the ecliptic plane) was demonstrated by John Goebel (2001, GP-B S0490 Rev. B). Note that the measurements of zodiacal light Goebel considered, taken from Leinert *et al.* (1998, A&AS, 127,1), include the effect of all scattering of sunlight by dust, no matter how distant. According to Leinert *et al.*, small-scale irregularities exist at only the few percent level. Nevertheless, in principle, if they are sufficiently sharp-edged they could produce large brightness gradients in at least some directions. However, as long as the dust lies within a few astronomical units of the Sun, any such features would be carried across the field of view of GP-B within a few days, and hence would not contribute significantly to the GP-B relativity signal. On the other hand, the effect of dust lying much closer to IM Peg than to the Sun would not be reduced in the same way.

Regardless of distance, since the field of view of GP-B is only ~1′ in radius, only dust within that angle of the line of sight to IM Peg can scatter light directly into the GP-B detectors. Since there is no star much brighter than IM Peg that is closer to it on the sky than α Peg (V = 2.5, d = 43 pc), about 3° away, and no star brighter than V ≈ 6 within at least 10′, we believe that it is very unlikely that any star other than IM Peg can illuminate any such dust brightly enough to significantly affect the GP-B pointing. [Alas, we don't see any easy way to prove that this is so. Perhaps we could in the future query some star catalog to show that the sum of the illumination by all catalogued stars is insignificant for GP-B, even for a sharp edged volume of dust ~1′ in size, whether optically thick or thin. We would still have to separately consider the illumination by the distant galactic disk and the galactic core and bulge, too. To first approximation, we can assume that the galactic disk is optically thin, infinite, and homogeneous, so it illuminates the whole Galaxy to about the same degree, allowing us to use the local value. The nearly optically thick shells surrounding certain carbon stars that have high mass-loss rates provide probes of the ambient light in certain specific locations (e.g., IRC+10216, Mauron and Huggins 2000, A&A, 359, 707).]

From here on we therefore consider only the case of dust illuminated by IM Peg itself. (If such dust exists, it would constitute a so-called reflection nebula.) The effect of such dust on GP-B depends both quantitatively and qualitatively on the geometrical relationship between the dust, the star, and Earth, in particular, on the angle of deflection between the emitted and scattered light rays, i.e., on the angle between the vector from the star to the dust and the vector from the dust to the GP-B spacecraft.

One might at first think that brightness of the dust so illuminated would vary nearly in proportion to the that of IM Peg, and hence that its effect on the pointing would be a

nearly constant offset on the sky and therefore not a serious problem for the GP-B mission. However, because the relatively cool and dark photospheric starspots that are thought to be responsible for the photometric variation of IM Peg are likely not uniformly distributed across the surface of the star, the brightness ratio need not be constant. In fact, it is plausible that, even when averaged over the entire GP-B mission, the trend in the brightness ratio will be as large or larger than the trend in the brightness of the star, relative to its mean brightness, as seen from Earth over the same period. We present the evidence in favor of this conclusion below.

(For completeness, we note here that two other effects could also lead to temporal variations in the brightness ratio of a star and its own reflection nebula. First, since the ray path from the star to the solar system of scattered light will be longer than the path of direct light, the scattered light is proportional to the brightness of the star at an earlier time than the time at which the direct light was emitted. For example, for light from IM Peg that is scattered just once and by 90°, and yet still within the field of view of view around IM Peg, the added path length is up to ~0.028 pc, or 0.090 light years. But since the corresponding delay is much less than the duration of the GP-B mission, the resulting contribution to the trend in the brightness ratio will likely be much smaller than the contribution considered below. Second, it is conceivable that the dust itself varies in time, due perhaps because it is non-uniformly distributed around some orbit about IM Peg, but we regard this possibility as being too unlikely to merit further consideration.)

The light detected by GP-B that was scattered by dust in any given volume not exactly between GP-B and IM Peg was originally emitted from a different hemisphere of the star than the one at that time visible to GP-B. The difference depends on the directions of GP-B and the dust as seen from the star. Because the autocorrelation time of the time-dependent spot distribution is much longer than the stellar rotation period (Strassmeier *et al.* 1996, A&A Supp., 125, 11; Henry, 2002, priv. comm.), during a complete rotation the difference in the relative brightness of IM Peg as seen from two different directions will at least partially average out. However, it will average out completely only if the two directions are equally displaced from the spin vector of the star. The worst case for GP-B that comes to mind would occur if the inclination of the spin axis with respect to our line of sight is close to 90° and if the brightening of one polar hemisphere of the star is often accompanied by the dimming of the other. How plausible is such a scenario? Based on indirect arguments, the inclination has been estimated as 55°-90° (Lebach *et al*. 1999, Apj, 517, L43) and 65°-80° (Berdyugina, Ilyin, & Tuominen 1999, A&A, 347, 932). Thus an inclination above 70° is probable, and the 90° scenario can serve as a useful simplification that only modestly overestimates the plausible long-term rate of change of the illumination of any dust by IM Peg. Furthermore, the multiyear changes in brightness of IM Peg might well be due to changes in polar or high latitude spots, which need not be identical in both hemispheres. On the other hand, we know of no reason to expect that the brightness of the two polar hemispheres would anticorrelate. To the contrary, on the Sun, sunspot activity is highly correlated between its two polar hemispheres. More relevant, though, is the behavior of the large-scale solar field, as perhaps best reflected in the distribution of coronal holes, which have been suggested as the closest solar analog to

the polar spots of RS CVn variables. The data suggest that, while there are some asymmetries in the distribution of coronal holes in the two polar hemispheres (Hofer and Storini 2002, Solar Phys., 207, 1), the distribution shows no sign of any anticorrelation between them. For the purpose of estimating a plausible bound on the relativity test error due to dust near IM Peg, we propose that one may regard the brightness variations of the two polar hemispheres as independent.

Consider, therefore, the simple case in which the inclination is 90° and the two polar hemispheres each have a uniform surface brightness which varies in time, independently of that of the other one, but with the same variance. The variance (in magnitudes) of the illumination of the dust over one pole would be twice the variance seen from any point over the equator, including from Earth. Consequently, it might seem reasonably conservative to bound the rate of change of the rotationally averaged magnitude difference of IM Peg as seen from any direction (even on the stellar rotation axis) at about $\sqrt{2}$ times the peak rate seen from Earth. However, a larger bound is required to allow for the possibility that the brightness changes seen from Earth are due mainly to surface brightness changes in high-latitude spots on IM Peg, which are highly foreshortened when viewed from Earth, and hence relatively weak in reducing the observed integrated stellar luminosity.

Since the best available spot maps of IM Peg (Berdyugina *et al.* 2000, A&A, 360, 272) indicate the presence of spots mainly between 30° and 80° latitude, and since other authors (e.g., Vogt *et al.* 1999, ApJS, 121,547) infer that RS CVn's generally have polar spots that extend at least 10° or 20° from each pole at all times, it seems implausible that the observed photometric variation of IM Peg ever arises mainly from spots at latitudes above, say, 60°. Consequently, we consider it unlikely ($p \sim 0.05$, say) that either the rms or the peak rate of fractional change in illumination along the spin axis is more than twice the rms or peak rate of change, respectively, of the rotationally averaged luminosity toward Earth from that hemisphere. Thus we suggest that any inferred upper bound on the expected effect of asymmetrically distributed dust on GP-B should allow for a rate of change in the illumination of the dust up to $2\sqrt{2}$ times the upper bound assumed for the rate of change of IM Peg brightness seen from Earth. For the purpose of computing the plausible effect on GP-B of stellar companions in the telescope field of view it has been agreed to take the latter bound as 5%/yr (see Appendix D). Consequently, for the purpose of computing the magnitude of the worst-case GP-B guiding error due to dust we take 15%/yr as the maximum plausible rate of change in the illumination of the dust (averaged over a stellar rotation period). However, since in the case under consideration there will be a 50% correlation between the polar brightness and the rotationally-averaged equatorial brightness seen from Earth, we take the maximum plausible rate of change the magnitude difference between the star and the integrated magnitude of the dust to be ~10%/yr. In any case, because the rate of change of the illumination of any given volume of dust is not necessarily highly correlated with the rate of change in stellar brightness seen from Earth, even after the latter has been monitored during the GP-B mission, much of the uncertainty in former will remain. That is, the worst-case astrometric error due to a change in the rotationally averaged illumination of the dust will

neither vanish nor be dramatically reduced, even if during the mission the trend in brightness seen by GP-B is much less than 5%/yr

Now we turn to the observations bearing on the question of how much dust lies in the direction of this star.

(3) Estimated dust column density toward IM Peg

Schlegel, Finkbeiner, and Davis (1998, ApJ, 500, 525) have computed a whole-sky estimate of the column density of dust in the interstellar medium (ISM) from a combination of 100 micron IRAS data and 100 and 240 micron COBE/DIRBE data. The formal uncertainty claimed for the estimate in any given direction is 10%, with a resolution of 6.1′ (FWHM). For historical reasons, astronomers usually express the column density of dust in magnitudes of reddening, E(B – V), which is defined as the difference between the increase in the apparent magnitude (i.e., the extinction) of any object in B band due to the ISM between the object and Earth and the extinction of the same object in V band. The E(B - V) is known to be proportional the optical depth of the dust at any given visible or near IR wavelength along almost all lines of sight, excluding those passing through dense clouds (Mathis 2000), which cover just a very small fraction of the sky. On average, extinction in V is generally found to be 3.1 E(B – V). The wavelength dependence is monotonically decreasing with wavelength across the GP-B passband (but not nearly so steeply as with a Rayleigh law). The table given by Mathis shows that at 700 nm (R band) the absorption is only 75% of that in V band, and at 900 nm (I band) only 48%. For dust illuminated by IM Peg, the number of scattered photons that will be detected by GP-B is perhaps best estimated assuming a mean extinction of ~2 E(B – V). (However, for any dust within ~1″ of IM Peg, it is also true that the shorter wavelengths contribute relatively more to the normalized GP-B pointing signal. For such dust, the nominal value for V or R band probably yields the better estimate of the induced pointing error, i.e., the estimate closer to that obtained from the integral over the entire GP-B passband of the detector currents due to the dust.)

The Schlegel *et al.* map shows a faint dust feature several degrees long extending over IM Peg, possibly associated with the brighter region ~4° to ~8° from IM Peg which is also a known high-latitude molecular cloud complex. Molecular clouds, unlike the more ubiquitous IRAS cirrus, often have detectable small dense spots, which could well have dust column densities that vary significantly on arcsecond to arcminute scales, and hence could more significantly affect GP-B pointing. The IRAS data do not clearly suggest whether the faint dust feature is actually associated with the known molecular cloud. However, circumstantial evidence suggests that it is: The localized region that forms a distinct peak in the 100 micron map 1° southwest of IM Peg, and near the midline of the dust feature, has been detected in emission in the 115 GHz molecular line of CO (see below) and resolved into two spots about 0.2° apart. The Doppler shifts of the emission line imply radial velocities of -9.5 km/s and -10.0 km/s. These values are consistent with a physical association with the molecular cloud complex, since the complex exhibits

radial velocities in the range -10 km/s to -1 km/s, with a mean of -5.7 km/s (Dame 2002, priv. comm.). In any case, the reddening in the direction of IM Peg itself (with a resolution of 6.1′) is 0.092 ± 0.015 mag. (The uncertainty represents the standard error as derived Schlegel *et al.* based comparisons between the observed and predicted colors of a sample of galaxies.)

(4) Scattering by a dust sheet near IM Peg

What amount of light could be scattered into the GP-B detectors by this dust? The worst case for GP-B that comes to mind would occur if the dust has a local maximum that is physically associated with IM Peg. We will address this possibility in the next section. Here we consider the case more strongly supported by the IRAS data: namely that the dust column near IM Peg varies mainly on a scale of order 1°. In that case, the most plausible cause of an asymmetry is that the dust is localized in one or more sheet-like structures, at least one of which near IM Peg is inclined with respect to the plane tangent to the sky at IM Peg. Such a configuration could be expected to produce highly asymmetric nebulosity in the GP-B field of view, if the star and the point on the sheet closest to it were separated on the sky by less than the diameter of the field of view; at the distance of IM Peg this angular diameter corresponds to a linear separation of ~10^4 A.U., or 0.05 pc. Admittedly, such a small astronomical distance requires a (random?) spatial coincidence that might reasonably be assigned a probability of only 0.001 to 0.01, even allowing that in the model of Sfeir *et al.* the edge of the Local Bubble appears to be somewhere within about 10 pc of IM Peg. Nevertheless, to get an order of magnitude estimate of the amount of light that would be scattered by such a structure, we consider next a toy model in which all the observed dust lies in an infinite, thin, plane sheet.

The 0.092 mag value for E(B - V) suggests that even if nearly all of the extinction occurs in our hypothetical sheet, the extinction through the sheet in R band is only ~0.18 mag along our line of sight. If the sheet is inclined to the plane of the sky at an angle i_s, the extinction normal to the sheet is ~0.18 mag * (cos i_s). To derive an order of magnitude estimate of the GP-B detector current due to scattered light, rather than consider a distribution of angles i_s we will take i_s to be 60°, the median value for an ensemble of planes with a uniform distribution of orientations. For this inclination, the inferred extinction normal to the sheet is 0.09 mag, and the corresponding transmission coefficient is $10^{(-0.09/2.5)} \approx 0.92$. Moreover, the extinction is the combined effect of both scattering and absorption. The ratio of the two is unknown, but 1:1 is plausible given the range of albedos of natural materials (Michael Jura 2002, priv. comm.). For this ratio, only a fraction 0.04 of normally incident light would be scattered. More generally, if the angle of incidence of the starlight on the sheet is denoted i, the fraction of starlight $f(i)$ that is scattered is $f(i) \approx 0.04/(\cos i)$, as long as $f(i) << 1$. In this idealized model, about half of the light scattered by the dust originally enters the dust sheet at grazing angles of incidence for which $f(i) \approx 0.5$. However, as seen from Earth, such scattered light will be spread much more widely across the sky than the scattered light for which the angle of incidence had been less than, say, 60°. (This relationship follows from the fact that, as

long as the star is more than a few stellar diameters from the sheet, all the light with grazing angles of incidence to the sheet strikes the sheet outside the circular region of the sheet lying closest to the star on the sky.) Consequently, unless the separation of the sheet from the guide star is very improbably small (an event with cumulative probability <0.001), all the light with grazing incidence, for which $f(i) \approx 0.5$, will, when scattered, lie outside the GP-B field of view, and hence not affect the spacecraft pointing. We therefore can ignore all such light with grazing incidence upon the dust sheet as we estimate the size of even the worst-case error. More specifically, for simplicity we shall consider only light with $i < 60°$, which is half of all the light entering the dust sheet, and one fourth of the total light output of the star. (For the moment we also ignore the cool spots on the guide star, which lead to corrections to these fractions that are likely just a few percent, and are almost certainly less than a factor of two.)

With these restrictions, we can now derive an order of magnitude estimate of the worst-case total GP-B detector current due to scattered light as a fraction of the current due to light direct from the guide star. If there were no factor of $1/(\cos i)$ in $f(i)$ above, the fraction of the light from the star that would enter the dust sheet with $i < 60°$ and then be isotropically scattered would be $0.04/4 = 0.01 = 1\%$. But it is readily shown that the mean value of $1/(\cos i)$ in the solid angle with $i < 60°$ is $2 \ln 2 \approx 1.4$. Thus we conclude that, if a thin flat layer inclined to the plane of the sky by 60° contains all the dust in the direction of IM Peg, ~1.4% of its total luminosity in R band will be scattered from the region of the dust sheet for which $i < 60°$. Under the plausible approximation of isotropic scattering, this region is also that with the highest surface brightness when viewed from any angle. Moreover, one consequence of restricting our analysis to light with $i < 60°$ is that for the assumed inclination of our dust sheet, all of this light will appear in the sky on one side of the guide star. (For example, if the sheet lies behind IM Peg and is oriented so that it recedes from us toward the east, then all of this brightest region will lie to the west of the guide star.) Nevertheless, the magnitude of the change in the effective guide point of GP-B will depend upon the separation of IM Peg from the sheet. But as long as the distance on the sky between the guide star and the point on the sheet closest to it in space is less than 0.5′, nearly all of this region will lie within 1′ of the guide star, and hence fall inside the field of view of GP-B. (Neither an exact or numerical integral of the brightness of the scattered light on both sides of the star has been done, but we expect that such a calculation would yield much less than 50% correction to simple calculation presented here. Moreover, in light of the many simplifying assumptions in our toy model, such a calculation is not warranted.) Since 0.5′ = 0.00015 rad, at the 95 pc distance of IM Peg, the 0.5′ maximum separation requirement will be met as long as the separation of the dust sheet from IM Peg along the line of sight is less than 95 pc * (0.00015 tan 60°) = 0.025 pc. Allowing, as we did above, that the radial distance to the edge of the Local Bubble in the direction of IM Peg is within about 10 pc of the distance to IM Peg, our nominal separation requirement might be met with a probability of roughly 0.0025. (We can safely ignore the approximately 30-fold smaller probability that the dust will be so close to IM Peg that most of the scattered light will appear to come from within 2″ of IM Peg, and hence offset the effective guide point significantly less than it otherwise would.) If we take into account that the inclination, i_s, of the dust sheet should be less than 60° half the time, then our rough estimate of the probability that the

percentage of IM Peg light scattered into some "side" of the GP-B field of view exceeds 1.4% will be 0.0013, or 0.13%. For present purposes, we will consider this probability close enough to the 0.27% probability level of our desired (3σ) worst case that we may regard the 1.4% level of scattered light as a reasonably close approximation to the worst-case level for our toy model.

To obtain the corresponding error, we need to find the roll-averaged pointing offset due to this scattered light. This offset will tend to be somewhat less than that due to a hypothetical background star in the field whose total detector current is 1.4% of that of the guide star, because the scattered light is spread out. If we approximate the shape of the bright patch as a semicircle of 1′ radius (i.e., as a step function of displacement in some direction), then, according to Appendix D, the reduction factor will be $2/\pi$. On the other hand, we concluded in section (2) that the mean rate of change over one year of the ratio of scattered to direct light could plausibly be as much as 3 times the rate of change in the brightness of IM Peg historically seen from Earth. Here, we need to make a crude calculation based on a guess at the median correction factor. Given the uncertainty in the inclination and spot distribution of IM Peg, and the arbitrary orientation of its spin axis with respect to the inclination of the dust sheet, we believe that a factor of 1.5 correction is reasonable. After all, if the point on the dust sheet closest to IM Peg happens to lie over the same stellar latitude as does the Earth, rather than over one of its rotation poles, then the roll-averaged ratio of scattered light to direct light would be approximately constant. (Even in that special case, a change in the relative brightness of the two polar hemispheres of the star would still cause a change in the centroid of the nebulosity on the sky. Nevertheless, this change would not cause a guiding error larger than that due to the worst-case effect of the changing integrated brightness of the nebulosity.) Thus the two correction factors, 1.5 and $2/\pi$, nearly cancel, and the worst-case effect of scattered light in our model is approximately the same as the plausible error due to a star contributing 1.4% of the total detector current of the guide star. If, as shown in Appendix D, a star yielding a total detector current equal to 0.00044 times that of the guide star can cause an offset to the effective guide point of 1 mas, corresponding to a plausible error in the proper motion of the effective guide point of 0.05 mas/yr, then the worst-case guiding error due to a dust sheet is found to be approximately 0.05 mas/yr * 0.014/0.0044 ≈ 1.6 mas/yr. (We have ignored the color correction, in effect assuming that the nebulosity is the same color as IM Peg. However, the extinction of the dust, and perhaps also its scattering, is most likely significantly weaker toward longer wavelengths, suggesting that the color correction is not truly negligible, but rather decreases the worst-case error by a factor of up to ~2.) Since the 1.6 mas/yr value represents the two-dimensional error, for each coordinate one can take the worst-case error to be a factor of $\sqrt{2}$ smaller, or 1.2 mas/yr.

Thus, if even 10% of the dust in the direction of IM Peg lies in such a thin sheet at the worst-case distance from IM Peg, then the resulting nebulosity could cause a significant problem for GP-B, on the order of 0.1 mas/yr. Furthermore, a gradient in a continuous three-dimensional dust distribution is, in a sense, just a generalization of this toy model. Inspection of the map of dust column density in Schlegel *et al.* suggests that the dust is actually quite patchy in the vicinity of IM Peg, with rms variations of at least 10% on

scales from 6′ to 2° within 3° of IM Peg. It would appear that unless some limit on such gradients can be justified, an observational limit is needed. Visual and near IR limits can be obtained from our HST images or from planned ground-based coronagraphic and adaptive-optics observations. Mid-IR observations can yield a bound the density of dust near IM Peg by placing a limit on the thermal emission it would give off to balance the energy absorbed from the visual and near IR light of IM Peg (since the albedo of the dust is unlikely to be larger than 0.9). We turn next to such observational limits.

(5) IRAS 12, 25, and 60 micron point-source photometry of IM Peg, which yields inconclusive evidence for dust near or within the IM Peg binary system;

The IRAS Point Source Catalog gives fluxes of 2.93 mJy, 0.625 mJy, and 0.233 mJy at 12 microns, 25 microns, and 60 microns, respectively. According to either Jura (1999, ApJ, 515, 706) or Plets *et al.* (1997, A&A, 323, 513), these data suggest an excess of 0.12 Jy at 60 micron compared to the flux that might have been expected based on the 12-micron measurement. While most stars with such an excess are probably surrounded by one or more localized dust rings or shells, for an active RS CVn like IM Peg, the excess may be the result of an extended chromosphere that is optically thick at 60 microns but "optically thin at shorter wavelengths because the primary source of opacity is free-free absorption by the hot gas" (Jura, 2002, priv. comm.). A background galaxy might also be contributing to the 60 micron flux. Further doubt about the presence of dust is raised by the fact that the independent IRAS Serendipitous Survey Catalog does not show any excess at 60 microns. On the other hand, according to Jura, "the position in the Serendipitous Catalog is not very good, and the flux extraction algorithm may have suffered from this." Subsequently, more sensitive observations at 21 microns obtained with the MIRSI camera at the IRTF have shown no sign of dust. This non-detection suggests that the IRAS flux density excess was caused by background dust (Giovanni Fazio, 2002, priv. comm.; see also section 7 below, concerning optical polarimetry of IM Peg).

What amount of light could be associated with the IR excess, even if it really were caused by dust? Jura estimates that the bolometric luminosity of the dust would be 3×10^{-5} times that of the star. Making the further assumption that the albedo of the dust is 0.5, he estimates that "a conservative upper limit" to the integrated optical brightness of the dust at 700 nm would be about 10^{-4} times that of the star. To compute a plausible but conservative experimental error, for sake of argument we take this value to be the true optical luminosity of the dust, and we allow all the nebulosity to be located in a compact region somewhere between 2″ and 45″ from IM Peg, where it would contribute the largest photon flux imbalance. From the data in Mathis (2000) for the typical ratios of interstellar extinction in the various bands, we can estimate that the (B – V) color of the dust will plausibly be 0.3 mag smaller than that of IM Peg itself. This color implies that the difference in V magnitude between the dust and the star is 9.7 mag and hence that the V magnitude of the dust is 15.5. We further allow for a 5%/yr secular variation in the dust-to-star brightness ratio. (That is, we assume that the surface brightness of IM Peg's

photosphere has sufficient anisotropy to allow that the ratio varies as much as historically observed variation of the star itself as seen from Earth.) Using the relation in Figure D-7, we find that the guide-point drift error due to this dust would be 0.016 mas/yr. For the worst-case error, we allow a fivefold increase in the optical luminosity of the dust, consistent with the more conservative assumption that the dust albedo is ~0.9 rather than ~0.5. We also allow for a 10%/yr secular variation in the brightness ratio, a value chosen somewhat arbitrarily to allow for 1.5 sigma levels in both the secular variation of the star during the mission and in the degree of anisotropy of the stellar photosphere. We thus estimate the worst-case error to be about tenfold larger than the plausible error. Even so, the worst-case value we derive is only 0.16 mas/yr, about an order of magnitude smaller than that allowed by our toy model of a thin dust sheet near IM Peg.

(6) Limits from CO maps on gas in the direction of IM Peg

Because regions of the interstellar medium (ISM) with high dust density are frequently found, as expected, to have high gas density as well, one possible sign of dense dust is the millimeter wavelength molecular spectral line emission commonly seen emitted by dense regions (molecular clouds) of the ISM. Tom Dame (2001, priv. comm.) checked the archives of his group's single-dish surveys of the 115 GHz 1-0 transition of CO in the general direction of IM Peg. He found a map of this region of the sky that showed no significant CO emission closer than 1° to IM Peg, but with relatively low sensitivity. In the fall of 2001 he used the CfA 1.2 m millimeter wave telescope to map, at greater sensitivity, a 1° by 4.5° region containing IM Peg and the nearest relatively bright compact feature in the 100 micron map, about 1° from IM Peg. (This new map sampled the sky every 1/8°, to nearly fully exploit the 8.4′ FWHM beam of the 1.2 antenna.) He detected significant emission only within ~0.2° of that compact IRAS feature. He then made a still more sensitive observation, pointing directly at IM Peg for 50 min. There was no trace of an emission line in the resulting spectrum, which had an rms noise level of 0.029 K in each 0.65 km/s spectral channel. What do these 115 GHz results imply for GP-B? Only that the 115 GHz data provide no evidence of any concentrations of dust not resolved in the IRAS 60 or 100 micron maps and that the gas associated with the dust inferred from the IRAS maps is probably largely atomic, rather than molecular. The argument, according to Dame (2002, priv. comm.), goes like this: "The usual assumption is that the velocity integrated CO intensity, W_{co}, is proportional to the H_2 column density, $N(H_2)$. In Dame *et al.* (2001, ApJ, 547, 792) we find

$$N(H_2)/W_{co} = 1.8 \times 10^{20}\ \mathrm{cm^{-2}\ K^{-1}\ km^{-1}\ s}$$

which is a fairly standard value." There is no rigorous way to decide the proper limits of integration over velocity, but all the existing detections of CO within several degrees of IM Peg lie at radial velocities between -11 km/s and 0 km/s. To estimate the amount of dust in this direction that is allowed by the 115 GHz observations, we make the plausible assumption that negligible amounts of molecular gas in this direction lie outside the above range of velocity. Thus the nondetection of CO at 115 GHz toward IM Peg

suggests that the column density of H_2 in that direction (including gas behind IM Peg) is no more than

$$N(H_2) = (11/0.65) * 0.029 \text{ K} * (1.8 \times 10^{20} \text{ cm}^{-2} \text{ K}^{-1} \text{ km}^{-1} \text{ s})$$
$$= 8.8 \times 10^{19} \text{ cm}^{-2}.$$

How much dust would be expected to be associated with this much H_2? According to Dame (2001, priv. comm.) the "standard conversion" (Bohlin, Savage, and Drake 1978, ApJ, 224, 132) predicts the interstellar reddening to be approximately

$$E(B - V) = (N(H)/10^{20} \text{ cm}^{-2}) / 58.$$

Taking $N(H) = 2\ N(H_2)$

$$E(B - V) = [2 * (8.8 \times 10^{19} \text{ cm}^{-2})/(10^{20} \text{ cm}^{-2})]/ 58$$
$$= 0.030.$$

In comparison, Schlegel *et al.* infer from IRAS data that the reddening in the direction of IM Peg is 0.092 mag, about threefold larger. The larger value indicates a larger column density of H (by mass), whether molecular or atomic, than is suggested by even the upper bound on the $N(H_2)$ column density from the CO observation. The most plausible explanation is that on this line of sight the lion's share of the hydrogen is atomic. This conclusion is only strengthened by the fact that it would be highly unusual if there were actually CO along any line of sight distributed in radial velocity across as much as 11 km/s, a fact which implies that the upper bound given above is very conservative in this regard.

(7) Evidence from IM Peg optical polarization suggesting dust

It is believed that the essential difference between clouds of gas and dust seen in reflected light as bright nebulae and those evident only due to their absorption of starlight is that the former are brightly illuminated by some exceptionally bright star close to them. Thus another way to look for evidence of nebulosity is to look for evidence of absorption by the same gas and dust. Dust sometimes reveals itself because it tends to introduce linear polarization into the light from stars, in which the intrinsic optical linear polarization is very small. This effect is thought to occur because the individual dust grains are aligned so that their longest dimension has a non-random distribution with respect to the local magnetic field. (The mechanism of this alignment is not understood, since no mechanism is known to be effective enough to overcome all the processes that tend to randomize the orientations. For a recent review of some of the operative mechanisms, see Efroimsky 2002, ApJ, 575, 886.) If the field direction does not vary too rapidly along the line of sight to the star, unequal scattering and absorption of light in the two different linear polarizations can create a net polarization. Distant stars in the galactic plane tend to have easily detectable polarization, as do those encircled by unusually large amounts of dust.

To see if there is an unusual amount of dust on the line of sight to IM Peg, we asked Pierre Bastien (U. Montreal) to add this star to his on-going program of measuring stellar linear polarization.

Bastien (2001, priv. comm.) detected ~0.1% linear polarization in the light from IM Peg near 766 nm, at a consistent orientation on the sky, in observations on three nights in August 2001. He regarded this detection not as a sign of circumstellar material, but rather as a result of the typical amount of widely-distributed interstellar dust seen on lines of sight to stars whose distances from us are comparable to that of IM Peg.

After Bastien's observations, Yudin and Evans (2002, A&A, 386, 916) published measurements of IM Peg polarization in BVRI from one night near minimum light in August 1994. They found linear polarization amplitudes consistent within their errors with a Rayleigh wavelength dependence (λ^{-4}). The B-band value was 0.72% ± 0.19%, while that in V was 0.23 ±0.10. Yudin and Evans write that the Rayleigh wavelength dependence is characteristic of only a minority of the RS CVn's studied so far. They go on to cite the suggestion by Scaltriti *et. al.* (1993, A&AS, 102, 343) that the Rayleigh wavelength dependence of the polarization of the RS CVn binary II Peg is due to scattering from either small dust particles or molecules. They also cite Scaltriti *et. al.*'s (1993, MNRAS, 264, 5) conclusion that optically thin circumstellar dust can explain the infrared excess of that binary, as well as in about half of all the RS CVn's whose visual and near infrared brightness they analyzed. The optical depths required are 0.004-0.005 at 10 microns, and the estimated distances of the dust from the primary star of the binaries are 35 to 60 times the stellar radius of the primary, i.e. 0.02″ to 0.04″. Note that for GP-B, even if all the extinction were entirely due to scattering, and all on one side of IM Peg, at such small angular separations from the star the scattered light would have an insignificant effect on the pointing. In addition, we note that it is not clear to us if the uneven distribution of spots on IM Peg could account for any or all of the polarization detected in these measurements.

(8) Search for H-α scattering in long-slit spectra of IM Peg.

When stars are embedded in particularly dense clouds of gas (and hence also dust) one of the more obvious signs of the gas can be H-α emission in within a few arcseconds of the star. For this reason we asked John Huchra to locate and examine long-slit spectra of IM Peg in the digital archives of the Whipple Observatory. Although a full numerical reduction of the spectra was not done, he reported (2001, priv. comm.) that no H-α emission was visible "to about 1% of the flux level of the star in the extraction aperture (about 3″ × 3″)." We have not attempted to convert this flux limit to a limit on the amount of dust near the star.

Appendix G – A catalog of stars near IM Peg and constraints on unknown sources. (jjk)

Designation	Error (mas/yr)	EW Error (mas/yr)	NS Error (mas/yr)	radius (arcmin)	RA (deg)	Dec (deg)	D RAcosDec (arcsec)	D Dec (arcsec)	B	V	R	I	ref
GPB-54+23	1.97E-02	-1.80E-02	8.01E-03	0.94	343.244464	16.847562	-53.90	22.91	15.74	14.96	14.52	14.05	a,b,c,d,f
GPB-23-25	1.95E-02	-1.28E-02	-1.47E-02	0.56	343.253042	16.834128	-23.02	-25.45	16.89	15.93	15.27	14.39	a,c
GPB+40-11	1.87E-02	1.80E-02	-5.05E-03	0.66	343.270556	16.838212	40.03	-10.75	22.35	18.75	16.45	13.77	a
GPB-54+01	1.26E-02	-1.26E-02	3.09E-04	0.85	343.244559	16.841548	-53.55	1.26	16.71	15.83	15.33	14.84	d
GPB+21-19	1.24E-02	9.05E-03	-8.55E-03	0.47	343.265400	16.835800	21.47	-19.43	17.63	16.68	15.75	14.75	e,f
GPB-31+59	8.67E-03	-3.84E-03	7.77E-03	1.10	343.250912	16.857695	-30.68	59.39	15.81	14.75	14.14	13.61	a,b,c,d,f
GPB-44+30	5.12E-03	-4.16E-03	2.98E-03	0.87	343.247142	16.849620	-44.26	30.32	17.54	16.87	16.37	15.62	a,d,f
GPB-20+16	2.46E-03	-1.85E-03	1.62E-03	0.43	343.253969	16.845769	-19.68	16.46	19.13	17.98	17.06	17.27	f
GPB-47+45	1.04E-03	-7.33E-04	7.35E-04	1.07	343.246323	16.853778	-47.20	45.29	18.70	17.63	16.90	16.03	a,d,f
GPB+11+22	6.73E-04	2.85E-04	6.10E-04	0.41	343.262405	16.847278	10.69	21.89	20.28	19.54	18.91	18.11	f
GPB+25+06	6.03E-04	5.83E-04	1.54E-04	0.43	343.266324	16.842933	24.80	6.25	20.16	19.36	18.68	18.98	f
GPB+01-61	4.89E-04	7.69E-06	-4.89E-04	1.01	343.259712	16.824306	1.00	-60.81	18.90	18.44	18.00	18.13	d
GPB-27+44	3.33E-04	-1.67E-04	2.88E-04	0.86	343.251950	16.853509	-26.95	44.32	22.07	20.54	19.40	18.24	a
GPB+15-35	3.21E-04	1.23E-04	-2.96E-04	0.63	343.263670	16.831478	15.24	-34.99	22.02	20.71	19.69	18.69	a
GPB+37-32	3.04E-04	2.28E-04	-2.01E-04	0.80	343.269845	16.832417	37.47	-31.61	22.07	20.68	19.62	18.57	a
GPB+16+42	2.93E-04	1.02E-04	2.75E-04	0.75	343.263970	16.852870	16.32	42.02	21.98	20.71	19.72	18.76	a
GPB+26-31	2.77E-04	1.73E-04	-2.16E-04	0.66	343.266648	16.832559	25.97	-31.10	21.82	20.70	19.80	18.96	a
GPB-34+11	2.48E-04	-2.34E-04	8.25E-05	0.57	343.250120	16.844345	-33.54	11.33	21.57	20.65	19.89	19.20	a
GPB+46-10	2.44E-04	2.38E-04	-5.42E-05	0.75	343.272167	16.838423	45.83	-9.99	21.67	20.67	19.86	19.11	a
GPB+21+37	2.43E-04	1.16E-04	2.14E-04	0.70	343.265200	16.851384	20.75	36.67	21.53	20.64	19.90	19.24	a
GPB+09+42	2.40E-04	5.07E-05	2.35E-04	0.71	343.262059	16.852828	9.45	41.87	21.51	20.64	19.90	19.25	a
GPB-26+39	2.22E-04	-1.20E-04	1.86E-04	0.77	343.252167	16.852017	-26.17	38.95	21.47	20.62	19.91	19.29	a
GPB+48+19	1.97E-04	1.82E-04	7.64E-05	0.83	343.272687	16.846528	47.71	19.19	20.92	20.42	19.95	19.60	a
GPB+51+28	1.69E-04	1.47E-04	8.43E-05	0.93	343.273562	16.848950	50.86	27.91	21.97	20.71	19.72	18.77	a
GPB+14+54	1.68E-04	4.18E-05	1.63E-04	0.93	343.263450	16.856184	14.45	53.95	21.92	20.70	19.75	18.83	a

Designation	Error (mas/yr)	EW Error (mas/yr)	NS Error (mas/yr)	radius (arcmin)	RA (deg)	Dec (deg)	D RAcosDec (arcsec)	D Dec (arcsec)	B	V	R	I	ref
GPB+29+44	1.68E-04	8.96E-05	1.42E-04	0.88	343.267578	16.853553	29.31	44.48	20.92	20.42	19.95	19.60	a
GPB+48+33	1.64E-04	1.33E-04	9.65E-05	0.94	343.272659	16.850409	47.61	33.16	21.95	20.71	19.73	18.79	a
GPB-12+54	1.44E-04	-3.00E-05	1.41E-04	0.92	343.256103	16.856148	-12.00	53.82	21.46	20.62	19.91	19.30	a
GPB+42+53	1.43E-04	8.66E-05	1.14E-04	1.10	343.271020	16.855789	41.70	52.53	22.08	20.25	18.93	17.54	a
GPB-38+45	1.18E-04	-7.36E-05	9.20E-05	0.96	343.248998	16.853673	-37.57	44.91	21.32	20.57	19.94	19.39	a
GPB+50+37	1.09E-04	8.61E-05	6.72E-05	1.01	343.273342	16.851581	50.06	37.38	21.93	20.70	19.74	18.82	a
GPB-08+59	1.05E-04	-1.39E-05	1.04E-04	0.99	343.257167	16.857506	-8.17	58.71	21.55	20.64	19.90	19.23	a
GPB+55+32	9.22E-05	7.87E-05	4.81E-05	1.03	343.274762	16.850167	55.18	32.29	21.87	20.70	19.77	18.89	a
GPB+61+20	8.96E-05	8.49E-05	2.84E-05	1.03	343.276512	16.846664	61.48	19.68	21.86	20.70	19.78	18.91	a
GPB-67-13	8.20E-05	-8.05E-05	-1.57E-05	1.14	343.239890	16.837715	-67.35	-12.54	20.41	19.55	18.84	18.20	a
GPB+42+47	8.13E-05	5.27E-05	6.19E-05	1.02	343.270992	16.854187	41.60	46.76	21.10	20.49	19.95	19.52	a
GPB-71-13	7.63E-05	-7.49E-05	-1.42E-05	1.16	343.239628	16.837606	-71.31	-12.93	20.40	19.48	18.72	18.03	a
GPB+65+14	7.47E-05	7.28E-05	1.69E-05	1.07	343.277523	16.845214	65.12	14.46	21.95	20.71	19.73	18.79	a
GPB+67-09	6.38E-05	6.33E-05	-8.48E-06	1.07	343.277959	16.838820	66.69	-8.56	21.80	20.69	19.81	18.98	a
GPB-13+64	5.85E-05	-1.15E-05	5.73E-05	1.08	343.255720	16.858912	-13.38	63.77	21.83	20.70	19.80	18.94	a
GPB+18+64	5.25E-05	1.38E-05	5.06E-05	1.10	343.264462	16.858856	18.10	63.57	21.83	20.70	19.80	18.94	a
GPB-69+21	3.50E-05	-3.34E-05	1.05E-05	1.15	343.240256	16.846953	-69.05	20.72	22.02	20.71	19.69	18.69	a
GPB-71-22	2.48E-05	-2.36E-05	-7.63E-06	1.20	343.239628	16.835064	-71.31	-22.08	22.07	20.62	19.52	18.42	a
GPB+55+48	2.19E-05	1.61E-05	1.47E-05	1.20	343.274817	16.854628	55.37	48.35	22.07	20.69	19.64	18.60	a
GPB+73+17	1.73E-05	1.69E-05	4.02E-06	1.19	343.279625	16.845806	72.68	16.59	21.66	20.67	19.87	19.13	a
GPB-26+70	1.73E-05	-5.87E-06	1.62E-05	1.24	343.252087	16.860639	-26.45	69.99	22.08	20.33	19.05	17.72	a
GPB+68-32	1.53E-05	1.37E-05	-6.67E-06	1.21	343.278450	16.832350	68.45	-31.85	22.04	20.71	19.68	18.66	a
GPB-80+36	1.29E-05	-1.17E-05	5.54E-06	1.42	343.237114	16.851328	-80.36	36.47	16.19	15.25	14.72	14.20	a,b,d,e
GPB-80-57	8.55E-06	-6.86E-06	-5.10E-06	1.58	343.237334	16.825475	-79.56	-56.60	19.00	17.05	15.55	13.93	a,d
GPB-50+57	7.53E-06	-4.83E-06	5.77E-06	1.24	343.245528	16.857106	-50.07	57.27	22.05	20.71	19.67	18.65	a
GPB-21+72	4.81E-06	-1.27E-06	4.64E-06	1.25	343.253670	16.861328	-20.76	72.47	21.78	20.69	19.82	19.00	a
GPB+46+62	3.98E-06	2.31E-06	3.24E-06	1.26	343.272167	16.858312	45.83	61.61	21.83	20.70	19.80	18.94	a
GPB-62+48	2.07E-06	-1.60E-06	1.31E-06	1.28	343.242250	16.854650	-61.87	48.43	21.76	20.69	19.82	19.02	a
GPB-84+50	1.94E-06	-1.65E-06	1.02E-06	1.63	343.234965	16.855043	-84.31	49.85	19.46	17.78	16.79	15.84	e

Designation	Error (mas/yr)	EW Error (mas/yr)	NS Error (mas/yr)	radius (arcmin)	RA (deg)	Dec (deg)	D RAcosDec (arcsec)	D Dec (arcsec)	B	V	R	I	ref
GPB+19-77	6.85E-07	1.59E-07	-6.67E-07	1.32	343.264789	16.819775	19.27	-77.12	21.34	19.50	18.17	16.77	a
GPB+88+01	6.66E-07	6.66E-07	1.08E-08	1.40	343.283842	16.841578	87.86	1.37	19.30	18.43	17.70	17.78	d
GPB-61+58	6.29E-07	-4.45E-07	4.45E-07	1.38	343.242470	16.857409	-61.08	58.36	22.11	19.93	18.41	16.77	a
GPB-22+80	4.48E-07	-1.13E-07	4.33E-07	1.38	343.253370	16.863492	-21.84	80.26	22.09	20.10	18.69	17.18	a
GPB-47+73	3.99E-07	-2.08E-07	3.41E-07	1.43	343.246431	16.861587	-46.82	73.40	19.40	19.06	18.66	18.01	a,d
GPB+01+81	3.62E-07	3.39E-09	3.62E-07	1.35	343.259656	16.863620	0.79	80.72	19.50	18.98	18.50	18.62	d
GPB+65-68	2.25E-07	1.51E-07	-1.67E-07	1.53	343.277412	16.822259	64.72	-68.18	22.07	20.46	19.27	18.04	a
GPB+75+31	2.24E-07	2.06E-07	8.79E-08	1.30	343.280225	16.849700	74.84	30.61	22.07	20.47	19.28	18.07	a
GPB+70+44	2.14E-07	1.79E-07	1.17E-07	1.33	343.278834	16.853375	69.84	43.84	22.07	20.50	19.32	18.13	a
GPB-54+61	2.14E-07	-1.38E-07	1.63E-07	1.33	343.244464	16.858156	-53.90	61.05	22.07	20.50	19.32	18.13	a
GPB+92+02	1.99E-07	1.99E-07	3.39E-09	1.47	343.285009	16.841614	92.07	1.50	18.98	19.28	21.08	20.82	a
GPB+90+37	1.72E-07	1.58E-07	6.71E-08	1.57	343.284570	16.851392	90.48	36.70	22.07	20.61	19.50	18.39	a
GPB+54-58	1.65E-07	1.10E-07	-1.23E-07	1.30	343.274545	16.825045	54.39	-58.15	22.07	20.64	19.55	18.47	a
GPB+71+56	1.65E-07	1.27E-07	1.05E-07	1.47	343.279242	16.856753	71.30	56.00	22.06	20.63	19.54	18.46	a
GPB+03-93	1.43E-07	4.06E-09	-1.43E-07	1.55	343.260200	16.815439	2.75	-92.73	22.05	20.71	19.67	18.65	a
GPB-83+10	1.41E-07	-1.40E-07	1.69E-08	1.33	343.236403	16.843850	-82.92	9.55	22.02	20.71	19.69	18.69	a
GPB-08+80	1.34E-07	-1.32E-08	1.33E-07	1.35	343.257114	16.863539	-8.36	80.43	21.96	20.71	19.73	18.78	a
GPB-90-06	1.24E-07	-1.24E-07	-7.94E-09	1.44	343.234464	16.839662	-89.90	-5.53	21.86	20.70	19.78	18.91	a
GPB-78-25	1.17E-07	-1.11E-07	-3.73E-08	1.32	343.237662	16.834159	-78.38	-25.34	21.74	20.68	19.84	19.05	a
GPB+46-64	1.16E-07	6.60E-08	-9.58E-08	1.30	343.272303	16.823328	46.32	-64.33	21.73	20.68	19.84	19.06	a
GPB-98+05	1.14E-07	-1.14E-07	6.61E-09	1.57	343.232142	16.842717	-98.26	5.47	21.72	20.68	19.84	19.07	a
GPB-75+52	1.06E-07	-8.56E-08	6.18E-08	1.48	343.238509	16.855662	-75.33	52.07	20.93	20.42	19.95	19.60	a
GPB+30-03	2.33E-09	2.31E-09	-2.67E-10	0.49	343.267850	16.840267	30.29	-3.35	92.05	31.69	200.58	94.19	a

Table G-1. Catalog of stars with 100 arcsec of IM Peg and plausible errors based on 5%/yr drift in IM Peg luminosity. The sum error terms are EW(RA): -0.005 mas/yr and NS(Dec): -0.025 mas/yr. References are **(a)** The APM-North Catalogue (McMahon+, 2000); **(b)** M2000:Bordeaux Carte du Ciel zone +11<dec<+10 (Rapaport+, 2001); **(c)** The HST Guide Star Catalog, Version 1.2 (Lasker+, 1996); **(d)** The USNO A2.0 Catalogue (Monet+, 1998); **(e)** Ratner, M.I. Private communication, 2002; **(f)** Analysis of HST Images, 2003.

Known sources

We compiled the star list in Table G-1 from catalog searches, analysis of HST images and photometry data from Arne Hendon at USNO. Based on a vector sum of all the contributions with all corrections prescribed in Appendix D, we obtain plausible error terms of -0.005 mas/yr and -0.025 mas/yr in the Right Ascension (EW) and Declination (NS) directions respectively. This assumes the plausible IM Peg luminosity drift of 5%/yr. Likewise, the worst cases based on 15% luminosity drift are -0.015 mas/yr in RA and -0.075 mas/yr in declination.

Unknown sources

We used HST images, acquired in 1997 (PI: Shapiro), to establish limits on the brightness of unknown sources as a function of radius. These images of IM Peg using WFPC2 indicate no sources on the central PC CCD at a level higher than 19th magnitude. The most sensitive level was obtained over most of the chip using the highly saturated 6 sec. Exposure with the F555W filter and 16 sec exposure with the F450W filter. Within about 1 arcsec of the core of the IM Peg image the high level of saturation significantly reduced the sensitivity so that less saturated exposures (0.16 sec with F555W and 20 sec with F336W) gave the best constraints. These images too became saturated within a radius of 0.35 arcsec. In this innermost range the 0.7 sec F336W gave the best constraint. All of these constraints were color adjusted to V assuming the IM Peg color indices. This is conservative since IM Peg is redder than most stars and the images used were in the V, B and U wavelength ranges. Later, to support the Monte Carle analysis in (Chandler and Ratner, 2003), a similar analysis was performed in the I spectral band using the 8 sec exposure with the F814W filter and the two 1 sec exposures with the F1042M filter. The results of these analyses are listed in Table G-2.

r_{min}	r_{max}	I-band limit	V-band limit
0.02	0.07	7.2	8.0
0.07	0.11	9.0	9.0
0.11	0.16	9.5	10.0
0.16	0.20	10.0	11.5
0.20	0.25	11.3	12.5
0.25	0.30	11.4	12.7
0.30	0.34	11.4	13.4
0.34	0.50	11.4	14.6
0.50	0.75	13.6	14.8
0.75	1.00	14.2	15.2
1.00	1.50	15.7	15.8
1.50	2.00	17.0	17.0
2.00	16	>17.5	>17.5

Table G-2. 1-σ upper bounds for other stars near IM Peg from HST images as a function of radius from the central core. Data from the PC-chip on the WFPC2 instrument were used to establish these limits

The results are based on statistical analysis of the brightness variations in annular regions of the images. These variations are dominated by the point response function (PRF) of the HST. The differences in the limits between the I-band and the V-band is the result of the difference in the HST PRFs in these two bands. These analyses were performed using Mathematica (see note below).

How likely is it that a bright star lies closer to the guide star than 0.4"? Using a plot of the Hubble Guide Star Catalog of a 29' x 23' region centered on the guide star, we estimate the frequency of stars brighter than 15th magnitude to be 3.1×10^{-5} arcsec^{-2}. The expected number of stars brighter than 15th magnitude within a random circle of 0.4" radius is only 3.1×10^{-5} arcsec$^{-2} \times \pi \times (0.4")^2 = 1.6 * 10^{-5}$. Thus the probability of such a star being present within 0.4" of the guide star can be ignored, even as a worst case. However, there is a far greater probability that the region near the guide star contains a companion star physically associated with it and hence not included in the probability computed above for a random location in this general direction. In fact, on the order of half of all known binary stars are apparently bound to additional stars to form a multiple system, most often a triple system. For example, The Bright Star Catalog (Hoffleit and Jaschek 1982, p. viii) contains 1715 double systems and 1036 multiple systems. In past decades each generation of improved detection techniques has significantly increased the percentage of bright stars known to be multiples, so the above statistics strongly suggest only that finding additional companions to a binary is a moderately likely event. Mayor and Mazeh (1987) specifically examined 25 known spectroscopic binaries (not visually resolved) for evidence that a third component orbits the known binary. They found spectroscopic evidence for such an additional component in 6 cases, and they infer that about 4 more have probably escaped detection. On the other hand, observations to date have not found any third component for the guide star, which is, in fact, a spectroscopic binary. The contributions of such an unresolved third body are accounted for in the error box 3.2.2.3 and (Chandler and Ratner, 2003). We take 0 mas/yr for the plausible and worst case error contribution from an unknown source which is not associated with IM Peg.

Note: The specific Mathematica runs for these analyses are available on the GP-B wing of the MSFC VRC (virtual research center) with file names:sep03psfdatI1.nb (inner radii, I filter), sep03psfdatI2.nb (middle radii, I filter), sep03psfdatI3.nb (outer radii, I filter), sep03psfdatV1.nb (inner radii, V filter), sep03psfdaV2.nb (inner radii, V filter), sep03psfdatV3.nb (inner radii, V filter).

Appendix H – Constraints on variability of sources (other than IM Peg) in the telescope field-of-view from observations and theoretical considerations.(mir)

The pointing signal due to light from sources other than the guide star depends on the spatial distribution of that light and the ratio between the photon detection rate from these sources and from the guide star. As long as this ratio is much smaller than unity, the pointing signal is proportional to it, and the total effect of light contributions from multiple sources on the relativity measurements is simply the sum of the responses to each source. If the rate of change of the pointing signal (in mas/yr, say) due to these sources is constant (in an inertial rather than body-fixed frame) throughout the mission, then an error of the same magnitude is introduced into the measured gyro drifts. (Any annual periodic component of this signal, depending upon its phase, could cause an error in the measured parallax, which does not lead to a relativity signal error, or to an error in the gyro readout scale factor, which does. The latter could conceivably be significant for the NS error, but further discussion of this possibility belongs under the heading of gyro readout scale-factor errors.) We expect that any photometric variation with spectral power only at periods less than half the mission length will largely average out in the relativity tests. However, it is not completely clear that this averaging will always occur. For example, any photometric variation that has a beat period of >~ 1 yr when beating against the 24.6 day guide star orbit period (or the spacecraft orbit period, and possibly others) might contribute much more error than other periodic photometric variations.

As long as the photometric variability of the other sources is statistically independent of the variation of the guide star (i.e., as long as there are no correlations among them), the errors caused by photometric changes in the guide star and by any given other source are additive to first order in those changes. The independence condition is met for all the stars in the field of view, which are too far from the guide star to have a physical connection (such as mass transfer) that could synchronize their brightness variations. We therefore can compute the plausible error by taking the RSS of all these independent plausible errors. We account for the error due to nebulosity (box 3.2.1.2) the same way, even though any nebulosity is likely to be scattered light from the guide star itself, because the uncertainty estimates in that box are, in fact, derived from our estimated bounds on the variation in the ratio of the nebular light to the light from the guide star. Note that errors proportional to the photometric variation of the guide star are considered separately in Box 3.2.1.3.

For 2.1.4.1 Known Stars

We compute the entries for this box based upon the measured magnitudes and estimated bounds on variability of the stars within 75″ of the guide star. Based on the calculation in Appendix D we take the offset in the roll-averaged effective guide point due to a star between 4" and 40" from the guide star to be 1.5 mas for a star of magnitude V = 14 and

identical color to the guide star. Color differences may contribute at most a factor of 2 as shown in fiure D-6. A full treatment requires a numerical integration over wavelength of the photon detection rate from each star by each detector. We consider such a calculation too laborious for present purposes. Instead, we note that the median wavelength of the photons detected from the guide star and from other known stars in the field of view will likely lie within the I band (750-980 nm at 50% transmission, Johnson 1965), or possibly R band (5850-790 nm), especially for the hotter stars.). We therefore compute the pointing errors based on the I band magnitudes of the stars known to lie in the GP-B field of view.

We take I = 4.3 for the guide star, based upon the differential photometry and comparison star brightness provided by Greg Henry (Tennessee State, 2000, priv. comm.) for September 1999 to January 2000. (During this period the mean V magnitude, estimated by eye from a plot he provided, was ~5.85. This mean is consistent with the long term mean value of 5.8 to 5.9 measured by Henry from 1987 to 2001, and also with the value V = 5.8 assumed in Appendix 2.1.[TBR].)

In I band, the brightest star within 60″ of the guide star appears to be the B=15.7, V=15.0, I=14.1 star lying ~56" WNW of the guide star in the CCD images taken and analyzed by Arne Henden (USNO, priv. comm. 2002). (The only star between 60" and 75" from the guide star, 66″ away, has I=13.6.) How much could the brightness of the I=14.1 star plausibly vary? The best indication known to us comes from a survey of high latitude field stars observed for five consecutive nights by Everett *et al*. (2002). They found that among the stars with V ~ 14 (for which the photometric precision of their study of more than 2000 stars with 13.8 < V < 16.5 was best) 17% varied in V by at least 0.001 mag. Everett *et al*. neither classify these slightly variable stars nor discuss their long-term variations. However, we can infer from Hall's (2000) tabulation of the numbers and types of the classical variables (with V variations at least ~0.3 mag) known as of 1990 that, in the vast majority of known variables, most of the variation is either periodic or quasiperiodic with periods of minutes to weeks. Our best guess (based on this inference and on the example of very slight variability observed in the sun) is that this characteristic applies also to most of the far larger percentage of stars found to be slightly variable by Everett et al. We thus infer that most of these stars would contribute much smaller errors to GP-B than if a star of the same maximum brightness in the field of view were changing brightness at a steady 0.001 mag/yr rate. It appears that the plausible long-term variation (measured in mag/yr) is more than 100 times smaller than that of the guide star (0.1 mag/yr), and the resulting upper bound is

$$0.001\text{mag/yr} \times 1.5\text{mas/mag} \times 10^{-0.4((14.1-4.3)-(14.0-5.8))} = 0.00034\text{mas/yr}.$$

This bound, although uncertain by approx. factor of 2, shows that plausible error is 2 or 3 orders of magnitude smaller than other plausible errors in the measurement of proper motion.

The worst case is not easily identified. Arne Henden (USNO, priv. comm. 2002) determined the UBVRI colors of the seven brightest stars within ~2' of the guide star

based upon CCD data from 4 nights spanning 49 days. For most of the stars, including the brightest star identified above, the rms variability about the mean (in V) was less than 0.05 mag. However, the photometric accuracy was poorer than normal (by a factor or ~10) for the second brightest star in I within 60" of the guide star, because this star happened to lie on a diffraction spike of the guide star image. (This spike is due to the fixed "spider" secondary mirror support structure of the equatorially mounted 1.0 m Hall telescope used for the observations.) For the worst case, we allow that this B=16.9, V=15.9, I=14.4 star lying ~34" SW of the guide star, could be a variable. Variation of even 0.3 mag over the 49 days is allowed by this data. Until further observations are obtained, this data set cannot rule out a constant rate of brightness change of even 2 mag/yr. However, so high a value is highly implausible. Summarizing their experience with photographic plates, which detect mostly stars varying at least 0.3 mag, Hoffmeister, Richter, and Wenzel (1985, p. 244-257) state that about one star in 400 is found to be variable on any time scale. Since this fraction happens to approximately equal our 0.27% probability for a 3-sigma worst case, we need to find the rate of long-term brightness change exceeded by the vast majority of these variables. Unfortunately, we have found no studies of the long-term variation of mean magnitude. We note that the ~0.1 mag changes (with 22-105 day periods) seen in the light curves of a small minority of RR Lyrae stars (which have 0.2-0.9 day periods) are well studied (Hoffmeister et al., 1985, p. 43). It seems highly implausible that rates of order 0.1 mag/yr in long term variability of a majority of variables could have escaped notice. We thus take that value as the worst case rate. (Clearly, however, it is desirable to bolster this statistical limit with photometric measurements of all known stars in the field of view at two or more well-separated epochs during the mission.)

Since the pointing signal due to each background star in the GP-B field of view depends upon the ratio of the photon detection rates from the background star to that from the guide star, the gyro drift error contributed by the 0.1 mag/yrchange identified above is the same as that due the existence of a nonvariable star of the same magnitude in the presence of a 0.1 mag/yr change in the guide star. The values given above imply that the I magnitude difference between the guide star and the brightest star is (14.4 - 4.3) = 10.1, and the corresponding proper motion error is

$$0.1\text{mag/yr} \times 1.5\text{mas/mag} \times 10^{-0.4((14.1-4.3)-(14.0-5.8))} = 0.034\text{mas/yr}.$$

Since the direction of this error is NE/SW, we adopt equal NS and EW errors, each reduced from this rate by $\sqrt{2}$. This bound is also highly uncertain, but implies that the worst case error due to photometric variations in the known stars in the GP-B field of view is an order of magnitude smaller than other plausible errors in the measurement of proper motion.

In closing, we note that there is a star 97" from IM Peg with V ≈ 16 that has recently been shown to be quite variable. It varies 0.5 to at least 0.7 mag with a period of 0.3 days (Arne Henden, USNO, priv. comm. 2002). However, we believe that the 97" separation from the guide star is large enough that this star should not add noticeably to the GP-B error.

Appendix L – Planned Optical Observations and Analyses (mir)

Table L-1. Summary of planned optical observations.

Improbable potential unknown	• **Observation** • **Instrument** • **Location** • **Schedule** • **Org/Institution(Observer)**	**Expected Result**
Large offset in proper motion of optical centroid due to an unseen third body	• Optical astrometry • 0.8 m/CCD & Astrometric Photometer • U. Pittsburgh, PA • ongoing, July-December • U. Pittsburgh(Gatewood)	Constrains the guiding error due to a third body with independent estimates of proper motion, proper acceleration, and guide star orbital parameters from optical observations as consistency check at the ~0.5 mas/yr level.
	• Spectroscopy • 0.6 m Coude aux. tel. • Lick Obs., CA • ongoing, July-December • UC Berkeley(Fischer)	Constrains probability of a third companion by establishing a 0.01-1.0 km/s bound on changes in the radial velocity of the center of mass of the binary.
Nebulosity due to an undetected nearby dust sheet	• Deep occulted imaging • 2.2m/occulted CCD • Mauna Kea, HI • fall 2003, fall 2004 • UC Berkeley(Kalas)	Nebulosity sensitivity to ~24^{th} mag/sq. arcsec at 2-90 arcsec separation, implying GP-B guiding error of <~0.03 mas/yr. Repeated to constrain error from changes in nebulosity.

-- Cont. --	• Polarimetry • 0.6m /P-filter/CCD • Lick Obs., CA • fall 2004 • UC, Berkeley(Kalas)	Sensitivity to polarized nebulosity to 24^{th} mag /sq. arcsec at separation <2 arcsec
Large changes in star spots	• Doppler imaging • Various spectrographs • Various observatories • Ongoing, spanning mission • ETH Zurich(Berdyugina)	Validate <0.02 mas/yr centroid drift during mission, with possible capability of correct-ion to 0.01 mas/yr.
Unusual variability of other sources in the field of view	• Field star photometry • 1.55m/CCD • Flagstaff Station, AZ • 10 nights spanning mission • USNO(Hendon) Also: • 0.8 m & 0.2m /CCD • U. Pittsburgh, PA • ongoing, July-December • U. Pittsburgh(Gatewood)	V ≈18 sensitivity ensures that undetected brightening of other sources in the GP-B ST FOV does not contribute more than 0.01 mas/yr guiding bias.
Unusual variability of guide star	• Aperture photometry • 0.4m T3 automated telescope • Fairborn Obs., AZ • Ongoing, May-June, Oct-Feb • Tennessee State U.(Henry)	$\Delta V < 0.01$ magnitude sensitivity ensures section 3.2.1 error boxes are validated during mission
	• Aperture photometry • 0.3m portable • Nashville, TN • During Fairborn down-time June-September 2004 • Tennessee State U.(Henry)	Assures coverage during Fairborn down time to support validation
	• Aperture photometry • Various telescopes • Various, US and Canada • Spanning mission, May-Feb. • AAVSO(various volunteers)	Improved coverage and redundancy increases confidence by indeterminate amount.

Table L-2. Planned analyses.

Improbable potential unknown	• **Analysis Method** • **Data** • **Schedule** • **Org/Institution(Analyst)**	**Expected Result**
Large offset in proper motion of optical centroid due to an unseen third body.	• Monte Carlo study • HST images, VLBI positions, IM Peg spectra, & statistical characteristics multiple-star systems • As warranted by VLBI results • CfA(Chandler)	Compute GP-B error statistics due to possi-bility that a third body exists that has not already been detected, yielding GP-B error of 0 mas/yr at 1-sigma confidence and <0.15mas/yr at 3-sigma confidence.
Nebulosity due to an undetected nearby dust sheet.	• Image analysis • Mt. Wilson adaptive optics CCD images from Turner • Fall 2003 • U. Penn. (Trilling)	Bound on nebulosity imbalance in annulus 0.21-1.1 arcsec from IM Peg allowing GP-B error < 0.1 mas/yr

Appendix M – Constraints on the difference between radio and optical proper motion from observational and theoretical considerations. (mir)

This appendix contains detailed discussion of the proper motion errors due to star spots and due to the possible drift of the radio source with respect to the center of mass of the IM Peg binary system.

The astrometric effect of star spots

The most useful constraint on the size of this effect is provided by a computation by Svetlana Berdyugina of the size of the orbit-averaged astrometric offset due to the spot distribution at eight recent epochs, as approximated by a series of published models (Berdyugina *et al*. 2000) of the brightness of the visible surface of the IM Peg primary. Each of these models was constructed by application of the Doppler mapping technique to spectroscopic observations of the star spanning at least one rotation of the primary, i.e., at least one orbital period. In support of the present study, she computed from these models a series of instantaneous offsets of the centroid of the star at 618 nm wavelength, in units of the radius of the primary. For each model, she then computed the average offset over a full rotation of the primary. (For constant spots this average would also be the average offset over any integral multiple of the orbit period.) The table below gives the results she obtained, as contained in a 12/3/02 email to one of us (MIR). Here the *y* axis is defined to be aligned with the projection of the stellar spin axis onto the plane of the sky. The orientation of this axis can be approximately determined by our VLBI observations, with a standard error of roughly 10˚, and perhaps also to similar accuracy by optical astrometry. The average *x* values are all zero because of the averaging over a rotation.

Season	Aver_*r*	Aver_*x*	Aver_*y*	Max_*r*	Max_*x*	Max_*y*
1996.72	0.0498	-0.0000	-0.0490	0.0933	0.0124	0.0933
1996.89	0.0623	-0.0000	-0.0622	0.1221	0.0068	0.1221
1997.62	0.0523	-0.0000	-0.0521	0.0705	0.0115	0.0704
1997.95	0.0310	-0.0000	-0.0286	0.0441	0.0266	0.0424
1998.53	0.0623	0.0000	-0.0616	0.1086	0.0167	0.1086
1998.75	0.0412	0.0000	-0.0400	0.0758	0.0189	0.0756
1999.57	0.0571	-0.0000	-0.0569	0.0786	0.0090	0.0785
1999.73	0.0635	0.0000	-0.0633	0.1024	0.0098	0.1024
Average shift for the eight models:						
	0.0524	0.0000	-0.0517			

The season-to-season change in average *y* represents a centroid drift that could cause the effective guide point to have a proper motion offset in the *y*-axis direction. Given the

limited (3 yr) duration of the observations, to be conservative we take as the plausible error the drift rate that, in one year, would span the full range of the tabulated values. Since the span of the offsets, in units of the radius of the primary, is –0.0286 to –0.0633, or 0.0353, and since the radius of the primary is estimated (Berdyugina *et al*. 1999) to be 13.3±0.06 solar radii = 0.062 AU, which subtends 0.65 mas at the 95 pc distance determined by our VLBI observations, this choice yields a plausible contribution to the effective guide point proper motion of 0.024 mas/yr. Further, given that the preliminary VLBI orbit orientation indicates that the spin axis is likely oriented approximately NW/SE, we take $1/\sqrt{2}$ times this value, or 0.017 mas/yr, for the plausible errors in both right ascension and declination.

The table sheds less light upon the worst-case error due to this effect. However, given that the star never dims by as much as a factor of two, and that it's spots probably cover no more than ~10% of its visible surface at maximum light (Berdyugina *et al*. 1999), the light centroid offset cannot exceed ~0.5 stellar radii at any time. It follows that its mean rate of change over one year cannot exceed ~0.65 mas/yr. Planned observations leading to Doppler maps at multiple epochs during the mission can be expected to reduce this worst-case error by at least an order of magnitude.

Radio drift with respect to the binary center of mass

As for the drift due to spots, the only component of the drift in the radio centroid that is likely to remain after averaging over an orbit period is the component parallel to the projection of IM Peg's spin axis onto the plane of the sky. (Note, however, that since the VLBI observations are sparse, we don't actually average the VLBI positions over any interval longer than a day. Rather, we fit to the VLBI positions the parameters of a circular orbit, in addition to those of parallax, proper motion, and constant proper acceleration.) There is no evidence suggesting that such a drift has been detected. On the other hand, it is quite plausible that there will be some drift due to changes in the magnetic field of the active primary component of IM Peg on multiyear time scales. The plausible magnitude of the drift is perhaps best estimated from that of the observed shorter-term motions of the radio emission centroid. On hour time scales, motions between 0.5 and 1 mas have been detected within 7 of the ~15 VLBI sessions during which such motions would have been detectable. On the other hand, no motions larger than ~1 mas have ever been detected (Lebach *et al.* 1999, Ransom *et al.* 2003, Bartel 2002). Furthermore, the postfit residuals reveal no detectable multiyear systematic motion. These facts are consistent with a source whose centroid, viewed in a frame rotating with the primary star, always remains within 1 mas, or ~0.75 stellar diameters, of some location in the binary system. (Admittedly, however, it is also possible that a relatively large systematic motion is not detected only because most of it is absorbed into the stellar proper motion and proper acceleration that are estimated from the VLBI positions.)

Although the stellar-latitude distribution of spots on IM Peg is expected to change cyclically with some period comparable to, or longer than, the 11 yr solar sunspot cycle, the size and symmetry of these changes about the stellar equator are essentially unknown (Berdyugina, 2002, priv. comm.). Further, the radio emission is thought to arise at heights of order one stellar radius above the photosphere, and hence to be shaped by

lower-order multipole components of the magnetic field than are the spots. It is, therefore, unclear if the latitude of radio emission, when averaged over a few years, varies as much as the similarly averaged latitude of the spots, or even if it varies at all. Moreover, in spite of large changes in the flux density, size, and shape of the stellar radio source from one VLBI session to another, the rms scatter of our VLBI position residuals is less than one stellar radius. It therefore seems improbable to us that the radio centroid, averaged over one session, is ever offset from the center of the primary by as much as a stellar radius. Somewhat arbitrarily, for the plausible error we allow that the centroid of the radio emission has a systematic sinusoidal motion with a projected peak-to-peak displacement of up to 0.34 mas, i.e., up to one-half the stellar radius, and a period of 20 yr. (Given that by the end of the GP-B mission we will have VLBI data on IM Peg spanning ~13 yr, periodic motions of the same angular amplitude but with significantly shorter or longer periods than 20 yr would contribute smaller errors.) For such a 20 yr periodic motion, the rms angular velocity on the sky with respect to the center of mass of the binary would be

$$\frac{0.34\,mas}{2\sqrt{2}\left(\frac{20\,yr}{2\pi}\right)} = 0.04\,mas/yr.$$

The VLBI data suggest that the projection of IM Peg's spin axis onto the plane of the sky points approximately NW/SE. Consistent with this currently rather uncertain orientation, and also with a completely random orientation, we take each component of the plausible error to be $1/\sqrt{2}$ times the value above, or 0.03 mas/yr.

For the worst case, we allow for motions with the same time dependence but 8 times the amplitude. This choice allows for a probability distribution with a wider tail than a Gaussian. A still higher value for the worst-case error would imply that the mean position of the radio emission during some years of our observations was displaced more than 2 radii (i.e., more than 1.33 mas) from the center of the primary. This implication is disfavored (but not logically excluded) by the small size (~0.5 mas rms) of the observed position residuals to the astrometric model fit to the entire set of VLBI positions of IM Peg. The VLBI observations thus give some support to our expectation that, in all years, the mean position of the centroid of the emission region remains within 2 radii of the center of the disk of the primary. Further, we are aware of no basis in current astrophysical models of the radio emission to expect such a large value. Thus, for the worst-case amplitude, we believe it is reasonable to allow for a peak-to-peak shift of 4 stellar radii, or 8 times the plausible amplitude. If we allow for an arbitrary orientation, we conclude that the estimated the worst-case (3σ) error in each coordinate is ~8 times the 0.04 mas/yr upper limit value adopted for the plausible error, or 0.3 mas/yr.